JOURNAL OF QUATERNARY SCIENCE (2025) 1–19 ISSN 0267-8179. DOI: 10.1002/jqs.3721

JQS Journal of Quaternary Science QRA Quaternary Research Association

Reconstructing the late Pleistocene glacial history of the Cairngorm Mountains, Scotland, using paired cosmogenic ^{10}Be and ^{14}C

SAMUEL E. KELLEY,[1]* ALICE M. DOUGHTY,[2] NATHANIEL LIFTON,[3] SIMON PENDLETON,[4] CORMAC O'BRIEN[1] and GRAEME WARREN[5]

[1]School of Earth Sciences, University College Dublin, Dublin, Ireland
[2]School of Earth and Climate Sciences, University of Maine, Orono, ME, USA
[3]Department of Earth, Atmospheric, and Planetary Sciences, Purdue University, West Lafayette, IN, USA
[4]Environmental Science and Policy, Plymouth State University, Plymouth, NH, USA
[5]School of Archaeology, University College Dublin, Dublin, Ireland

Received 20 December 2024; Revised 11 April 2025; Accepted 25 April 2025

ABSTRACT: Chronologic and geomorphic evidence of past glaciations is largely recorded in areas at relatively low elevation and/or landscapes defined by high glacial erosion. As a result, data from areas that did not experience significant glacial erosion and the highest elevation locations are lacking from reconstructions of past ice masses. Here, we use paired ^{10}Be and ^{14}C exposure dating on quartz derived from glacial erratics and bedrock to resolve past ice mass fluctuations across an elevation and geomorphic gradient in the Cairngorm Mountains of Scotland. We find that the highest elevation samples in our dataset, at 1140 m above sea level, yield ^{10}Be ages indicating 23 000 years of exposure and are at secular equilibrium for ^{14}C, indicative of a single period of exposure starting as a nunatak during the Last Glacial Maximum. Other samples from above 1000 m elevation produce ^{14}C exposure ages indicating deglaciation during the Bølling–Allerød Interstadial, while ^{10}Be concentrations display varying levels of inheritance due to local variations in glacial and non-glacial erosion. Samples from lower elevations indicate a Lateglacial moraine building event 15 000 years ago, coincident with the Wester Ross readvance, followed by a period of glacier retreat interrupted by moraine deposition at ~14 000 and ~11 000 years ago. This dataset reconstructs both thinning and marginal recession of paleo-ice masses within the Cairngorm Mountains across a >600 m vertical gradient during the most recent glacial–interglacial transition, demonstrating the utility of paired ^{10}Be/^{14}C exposure dating in ice mass reconstructions in areas of low glacial erosion, increasing the geomorphic diversity of chronologic data available for glacial reconstructions.

KEYWORDS: cosmogenic nuclide; geomorphology; Lateglacial; paleoclimate; Scotland

Introduction

Mountain landscapes in glaciated regions have long interested Quaternary geologists, as the deeply weathered bedrock at high elevations belies a landscape much older than the glacially abraded bedrock found at lower elevations (Ives, 1978; Sugden, 1978; Ballantyne, 1998; Briner et al., 2003). In some locations, boundaries between heavily weathered landscapes above and glacially abraded landscapes below define past glacier extent (Rootes and Clark, 2020); however, in other locations, the entire mountain landscape was glaciated with areas exhibiting subaerially weathered bedrock indicative of cold-based, minimally erosive, ice cover (Hättestrand and Stroeven, 2002; Davis et al., 2006; Phillips et al., 2006; Koester et al., 2021). This juxtaposition of geomorphic regimes highlights one of the challenges in reconstructing ice masses in areas of high topography. Traditionally, studies of mid-latitude glaciation have used geomorphology (Hall and Sugden, 1987; Kleman, 1994; McMartin et al., 2021) or cosmogenic nuclide abundances (Stroeven et al., 2002; Ballantyne et al., 2006; Phillips et al., 2006; Briner et al., 2014; Hall et al., 2024) to document landscapes that lack modification during the last glacial period. Yet, the majority of chronology (Clark et al., 2022; Hughes et al., 2022; Dalton et al., 2023) and ice flow constraints (Prest et al., 1967; Hughes et al., 2014; Margold et al., 2015) are derived from lower elevation landscapes. The scarcity of high-elevation Quaternary geochronology is likely because of a relative lack of suitable material for geochronologic techniques, as well as a smaller proportionally land area with respect to lower-elevation glaciated areas. Except for landscapes dominated by modern ice sheets, such as is the case in Greenland (Beel et al., 2016; Graham et al., 2019) and in Antarctica (Johnson et al., 2019; Nichols et al., 2019; Spector et al., 2020), where paleo and modern nunataks form a significant component of terrestrial records of past ice sheet change, the majority of data used in glacial reconstructions comes from low elevation regions that experienced warm-based ice cover. Chronologic constraints from higher elevation landscapes are needed to complement detailed glacial reconstructions based on lower elevation deposits to address outstanding questions, such as three-dimensional ice mass geometry, spatial responses to changes in climate (i.e., thinning vs. marginal retreat), and reconstructions of isostatic loading for forecasting relative sea level rise.

Research plan

To address the challenges of glacial reconstructions within mountain landscapes, we focused on the Cairngorm Mountains

*Correspondence: Samuel E. Kelley, as above.
Email: sam.kelley@ucd.ie

of Scotland (57.08 N, 3.65 W, max elevation of 1309 m a.s.l.), which is the largest contiguous area over 1000 m a.s.l. in Britain and Ireland, located within the maritime climate of the North Atlantic (Fig. 1). While a wealth of geochronologic and geomorphic data are available from the Cairngorms, and the wider Grampian Mountains, open questions remain regarding the three-dimensional picture of ice mass evolution since the last glaciation, which we aim to answer.

Research Questions:

(1) What is the timing of deglaciation for the high plateau?

(2) Did glacial ice disappear from the corries or the high plateau first during deglaciation?

Here, we use ^{10}Be exposure dating, in conjunction with paired ^{10}Be/^{14}C, from quartz extracted from bedrock and glacially transported boulder samples collected on the relatively high-elevation Cairngorm Plateau, nearby corries (cirques), and from lower-elevation valleys to investigate the timing and spatial pattern of deglaciation. Terrestrial cosmogenic nuclide dating (TCN) is a frequently used geochronologic tool for reconstructing spatiotemporal patterns of ice

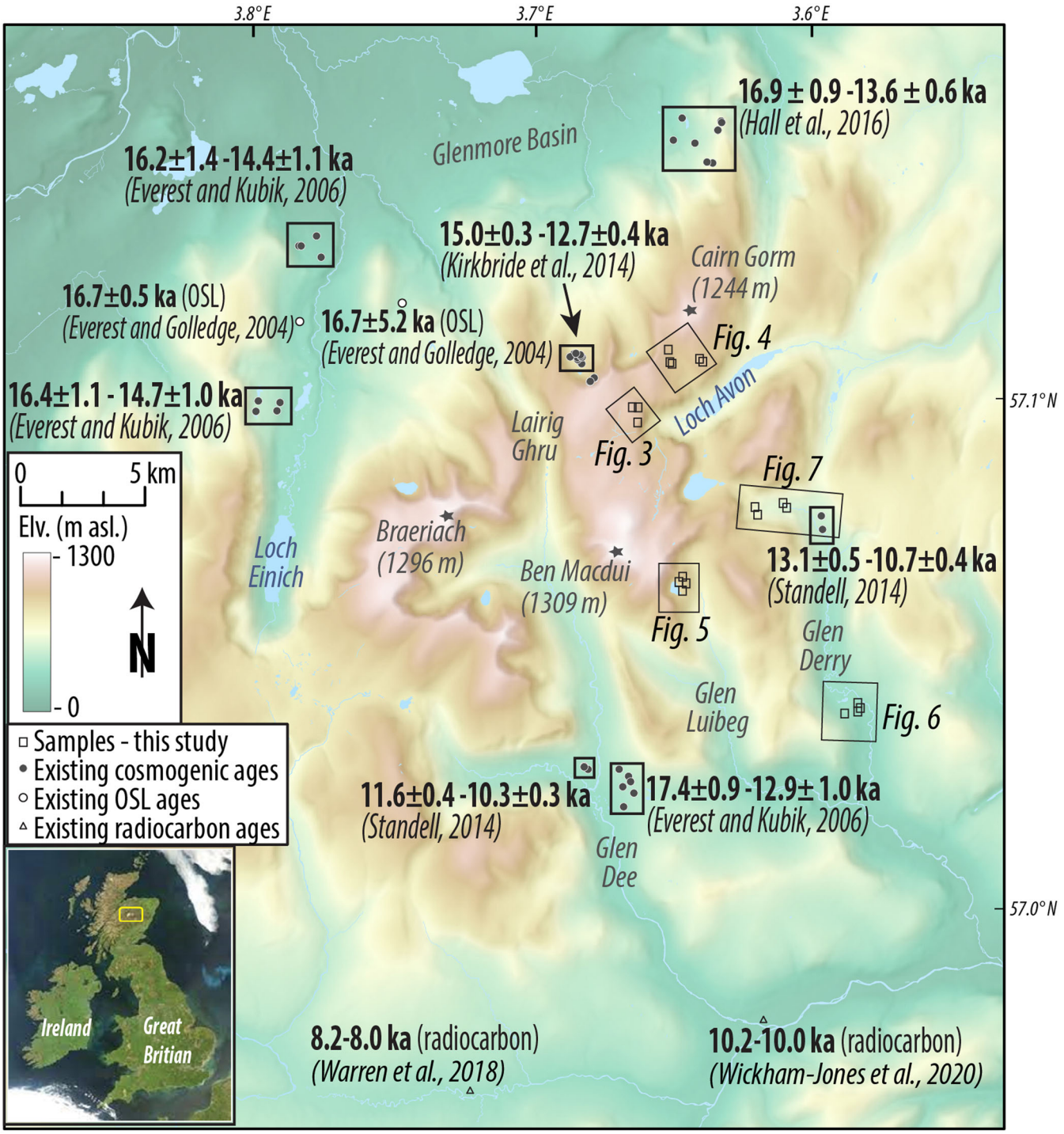

Figure 1. Map of the study area with key locations, existing chronology, as well as the location of sample sites for this study (open squares). All ^{10}Be exposure ages are recalculated from publications using the production rate calibration dataset of Borchers et al. (2016) and LSDn scaling (Lifton et al., 2014; Lifton, 2016). Data for all previously published cosmogenic exposure ages are presented in the figure and can be found in Appendix 2. The inset map shows the location of the study area within Britain and Ireland. Base map uses the Ordnance Survey terrain 50 DTM from https://digimap.edina.ac.uk/. [Color figure can be viewed at wileyonlinelibrary.com]

cover (Balco, 2011). Yet, in landscapes defined by minimally erosive glacial ice cover, or lacking ice cover, terrestrial cosmogenic exposure ages derived from commonly used cosmogenic isotopes, such as ^{10}Be, ^{26}Al, or ^{36}Cl, are often much older than the timing of regional deglaciation (e.g. Hall et al., 2024). These apparently 'old' exposure ages are due to nuclide inventories inherited from previous ice-free periods, which have not been fully removed due to insufficient glacial erosion. Our multi-isotope approach to examine the deglaciation of the Cairngorm Mountains uses a long-lived isotope, ^{10}Be (half-life of ~1.4 My), and a short-lived isotope, ^{14}C (half-life of 5.7 ky), to evaluate the past glacial history of this mountain landscape across three-dimensions. In using ^{14}C, we aim to determine the timing of deglaciation, while avoiding complications driven by inherited nuclides from previous interglacials seen in other studies (e.g. Phillips et al., 2006). A second possibility exists that our ^{14}C concentrations will be at secular equilibrium between production and decay ('saturation'), which typically indicates >25–30 ky (ca. five half-lives) of continuous exposure. This scenario could result from sites that were exposed as a nunatak during the most recent glaciation, or those that did not have long enough periods of glacial cover to allow previously accumulated inventories of ^{14}C to decay away. We use paired ^{10}Be and ^{14}C to yield insights into both the timing of deglaciation and landscape evolution.

Our new chronologic constraints, in conjunction with existing geomorphic mapping (Standell, 2014) and local paleotemperature reconstructions (Brooks et al., 2012), create a holistic picture of cryospheric change in the region from the end of the last glaciation through the earliest Holocene. The chronology generated will provide a three-dimensional view of the response of Cairngorm glaciers to Lateglacial (18–11.6 ka) and Holocene (11.6 ka–present) climate change. We note that this glacial reconstruction is in support of a wider interdisciplinary project investigating interaction between Mesolithic hunter-gatherers and the landscape of the Cairngorms; for more information about our archeological research, please see Butler et al. (2021, 2024).

Glacial geomorphology

The Cairngorms Mountains form the highest upland region in Britain and Ireland, underlain by a granite batholith emplaced ~400 Ma (Harrison, 1986). The region is characterized by high relief, resulting from repeated periods of selective linear erosion during glaciations (Fig. 1; Sugden, 1968; Rea, 1998; Hall et al., 2013). Glacial geomorphic mapping in the Cairngorms has largely been site-specific, with detailed studies on ice-dammed lakes (Brazier et al., 1998; Golledge, 2002; Standell, 2014) and specific paleoglacier systems (Rapson, 1983; Bennett and Glasser, 1991; Kirkbride et al., 2014). Two recent regional-scale mapping efforts were undertaken, one by Scottish Natural Heritage (Kirkbride and Gordon, 2010) and a second by Standell (2014). Mapping by Standell (2014), which builds from Sugden (1970), depicts a landscape defined at lower elevations by the Lateglacial retreat of local glacier systems and the preservation of relict terrain, exhibiting evidence of prolonged subaerial weathering at higher elevations. Valley and corrie systems contain numerous examples of glacial modification in the form of moraines, meltwater channels, and ice-molded bedrock, as well as postglacial features such as shorelines resulting from glacially dammed lakes, and glaciolacustrine deltas (Fig. 2C–D; Sugden, 1970; Brazier et al., 1998; Standell, 2014). In contrast, high-elevation areas largely lack evidence of glacial modification and contain large tors and extensive blockfields (Fig. 2a; Hall et al., 2013), as well as an absence of foreign erratics (Jamieson, 1908). Furthermore, ^{26}Al to ^{10}Be concentrations from samples collected from tors suggest great antiquity for portions of the plateau relative to lower elevation areas, with landscapes containing geochemical evidence for greater than 500 ka of exposure (Phillips et al., 2006).

The last glacial period

The timing of the most recent ice build-up in the Cairngorm Mountains is poorly constrained; for a more thorough treatment of this topic, see Ballantyne and Small (2019) or Scourse (2024).

Figure 2. (A) Tor near the summit of Cairn Gorm sampled by Phillips et al. (2006), view to the east. (B) Blockfield on the margin of Coire Raibeirt, view to the northwest. (C) Hummocky moraine is in the upper reaches of Glen Dee, view to the north. (D) Moraines fronting a Lochain Uaine on the eastern flank of Ben MacDui, view to the northeast, samples collected from this moraine in this study. [Color figure can be viewed at wileyonlinelibrary.com]

Evidence for the presence of glacial ice before the last glacial maximum (LGM) in Scotland primarily comes from ice-rafted debris found in marine cores. Core MD04-2882 from the Rockall Trough in the northeastern Atlantic contains material indicative of the early stages of the British Irish Ice Sheet (BIIS) after ~43 ka, with an increase in the material after ~35 ka (Hibbert et al., 2010). This indicates that conditions were favorable for the growth of tidewater glaciers in western Scotland, possibly within the Cairngorm, during marine isotope stage (MIS) 3 (60–29 ka; Voelker et al., 1997). Evidence of ice-free conditions comes from locations distal to the Cairngorms, such as Tiendland at ~32 ka (located ~70 km NW of the center of the Cairngorms; FitzPatrick, 1965) and at ~39– 32 ka Balgalss Burn (located ~120 km SSW of the center of the (Cairngorms; Brown et al., 2007), as well as from organic-rich sands at Tolsta Head that were overrun by advancing ice after ~33 ka (located ~200 km NW of the center of the (Cairngorms; Whittington and Hall, 2002). In total, fluctuations in ice cover appear to have occurred during MIS 3 in coastal and lowland Scotland, although no evidence exists to constrain mountain glacier survival in the Cairngorm.

During the last glacial period, the Cairngorms are believed to have acted as a regional ice-dispersal center for the larger BIIS, as evidenced by the lack of foreign erratics and radiating ice flow evidence (Bremmer, 1929; Sugden, 1970; Hubbard et al., 2009). This assessment is mirrored in recent modeling by Clark et al. (2022), which places an ice divide over the Cairngorms for much of the last glaciation. Geomorphic evidence, such as the presence of tors and blockfields on high ground within the Cairngorms, in addition to anomalously old terrestrial cosmogenic nuclide ages, likely due to nuclide inheritance, indicate the presence of sustained cold-based, non-erosive, ice conditions on high ground in central Scotland (Hall and Sugden, 1987; Phillips et al., 2006; Hall et al., 2013), and perhaps indicative of thin, non-erosive, local ice cover during the last glacial period (Merritt et al., 2017).

Cairngorm deglaciation

The recession of the BIIS toward the Scottish mainland began with the recession of the Minch Ice Stream as early as 30 ka (Clark et al., 2022), with recession onto North Rona around 28 ka (Everest et al., 2013). To the east of Scotland, the BIIS retreat in the North Sea Sector began by 23 ka, with separation from ice sourced in Scandinavia (Roberts et al., 2018; Clark et al., 2022). Separation of local Cairngorm ice and that of the larger BIIS is well constrained, with retreating Strathspey ice readvancing to form moraines along the northern slopes of the Cairngorms (Fig. 1; Everest and Kubik, 2006; Hall et al., 2016) between 16.9 ± 0.9 and 13.6 ± 0.6 ka (all exposure ages have been recalculated using the global production rates from Borchers et al. (2016) and the LSDn scaling scheme from Lifton et al. (2014) and Lifton (2016)). This timing of deglaciation is corroborated by minimum-limiting radiocarbon ages from Abernethy Forest, placing recession of ice before 15.1 ± 0.9 cal ka (Vasari and Vasari, 1968; all radiocarbon ages are recalibrated using IntCal20 from Reimer (2020)) and from a kettle hole near Loch Etteridge, to the west, which yields a calibrated basal age of 15.8 ± 0.6 cal ka (Sissons and Walker, 1974) and 15.5 ± 0.2 cal ka (Everest and Golledge, 2004). Recession of local Cairngorm sourced ice is estimated to have occurred by 15.8 ± 0.8 ka based on a single erratic believed to be free of inheritance located at 1156 m above sea level (a.s.l.) ~10 km to the east near the summit of Beinn a' Bhùird (Phillips et al., 2006). Exposure ages constrain the recession of the local glaciers into the main valleys on the Glen Einich moraines between 16.4 ± 1.1 and 14.7 ± 1.1 ka (Fig. 1; Everest and Kubik, 2006). Receding Cairngorm-sourced ice masses, in concert with the receding BIIS, blocked many drainages, leading to the impoundment of numerous glacially dammed lakes. While chronologic evidence is sparse, a pair of optically stimulated luminescence ages from the Lairig Ghru and Glen Einich constrain glacial lake formation to 16.7 ± 5.2 and 16.7 ± 0.5 ka, respectively, agreeing with the timing of separation of local Cairngorm-sourced glaciers from the larger ice sheet (Fig. 1; Everest and Golledge, 2004). Abundant evidence of glacially dammed lakes exists in the form of erosional shorelines and raised deltas in Glen Einich, the Lairig Ghru, Glen Derry, and Glen Luibeg (Brazier et al., 1998; Golledge, 2002; Everest and Golledge, 2004).

On the southern margin of the Cairngorms, the timing of deglaciation is not as well constrained as in the north. Radiocarbon ages from a kettle hole near the town of Braemar show ice had receded out of the upper Dee Valley by 14.9 ± 0.7 ka (Huntley, 1976). In Glen Dee, on the southern front of the Cairngorm Plateau, six cosmogenic ages from erratics located between prominent meltwater channels, possibly draining an impounded glacial lake, record an ice margin position well within the highlands between 17.4 ± 0.9 and 12.9 ± 1.0 ka (Everest and Kubik, 2006). Given the geomorphology of the site, an alternative interpretation of these ages would be that the two youngest ages in the dataset, 13.1 ± 0.7 ka and 12.9 ± 1.0 ka, result from the exhumation of boulders via glacial lake outburst believed to occur in Glen Dee during the latest Pleistocene (Fig. 1: Wickham-Jones et al., 2020), indicating the older ages in the spread are correlated ice retreat in the Lateglaical (17.4 ± 0.9 to 14.6 ± 1.0 ka; $n = 4$).

Younger Dryas and Holocene

A chironomid-derived summer temperature reconstruction from nearby Abernethy Bog (15 km north of the center of the Cairngorms) records a pronounced cooling of 5.6°C at ~14 ka, followed by cooling of 5.8 to 6.8°C during the early Younger Dryas (YD; Brooks et al., 2012). Work by Sissons (1979) placed the extent of glacier systems advancing into the upper reaches of some major valleys during the YD (12.9 to 11.6 ka; Steffensen et al., 2008), while Sugden (1970) suggested that YD glacier systems were restricted to high corries. More recently, Bromley et al. (2023) have suggested that the timing of ice expansion in Scotland may have preceded the YD, indicating landforms historically attributed to the YD formed in the earlier stages of Lateglacial. At the confluence of Glen Dee and Glen Geusachan, three exposure ages from boulders on hummocky moraines yield a mean age of 11.1 ka and a standard deviation of 700 years, constraining the recession of ice (Fig. 1; Standell, 2014). In Glen Derry, the recession of ice within a series of hummocky moraine fragments in the upper valley had occurred by 13.1 ± 0.5 ka, with further recession of ~300 m by 11.2 ± 0.4 to 10.7 ± 0.4 ka (Fig. 1; Standell, 2014). On the northern slope of the Cairngorm, in Coire an Lochain exposure ages from six boulders along a drift limit yield ages between 16.0 ± 0.6 and 13.5 ± 0.5 ka (Fig. 1; Kirkbride et al., 2014), with five younger ages of ranging from 15.0 ± 0.3 to 12.7 ± 0.4 ka derived from boulders inboard of the drift limit, constraining a Lateglacial ice margin position within the northern corries of the Cairngorm Mountains. Coring from the Lochain Uaine documents that the basin was ice-free by at least the middle Holocene, with no evidence of a neoglacial or Little Ice Age glacier (Rapson, 1983).

Methods

Cosmogenic exposure dating with ^{10}Be, ^{14}C

Twenty samples were collected for cosmogenic exposure dating from glacially transported boulders and prominent

bedrock outcrops at five sample sites within the Cairngorm Mountains. In descending elevation, the sample sites are as follows: (1) Fèith Budhie (three bedrock samples); (2) Coire Raibeirt (three bedrock samples and two boulder samples); (3) Lochain Uaine (four boulder samples); (4) Upper Glen Derry (four boulder samples); and (5) the Derry Dam (four boulder samples). Given the landscape dichotomy, with presumed cold-based non-erosive ice situated on the plateau (sample sites 1 and 2), and erosive warm-based ice in corries and valleys (sample sites 3, 4, 5), samples from the plateau were processed for both ^{10}Be and ^{14}C in an effort to overcome inheritance issues encountered in other studies (Phillips et al., 2006; Hall et al., 2024). Samples collected from Glen Derry are presumed to come from a more erosive glacial regime; thus, only ^{10}Be was extracted and measured from rock samples. Initial ^{10}Be results from Lochain Uaine indicated potential inheritance; thus, a subset of three samples from Lochain Uaine were processed for ^{14}C (Tables 1 and 3).

Sampling and documentation

Boulders and outcrops selected for sampling were prominent on the landscape, minimizing potential issues from snow cover. Samples were collected from the uppermost, flat surface using a battery-powered angle grinder, chisel, and rock hammer. Sampling avoided edges and areas of apparent erosion. The position and elevation of sample locations were recorded using a handheld Garmin GPS, as well as via a mobile mapping application containing a georeferenced topographic map. To confirm field measurements, all sample locations were checked using a 5 m DTM (Landmap, 2014) and high-resolution satellite imagery (Microsoft, 2025), where, in most cases, the sampled boulder/bedrock outcrop is visible. Sample thickness was estimated in the field and then measured in the lab before physical processing. Topographic shielding was measured for each sample in the field using a compass and clinometer, with the exception of GD2101, 02, 05, 06, and LU2102, where shielding was estimated using the profile generation tool in Google Earth due to low cloud cover at the time of sampling. A topographic shielding factor was calculated using the online calculator http://stoneage.ice-d.org/math/skyline/skyline_in.html. To confirm that our profile generation method was consistent with our field measurements, we also calculated shielding using Google Earth for sites where shielding was measured in the field. Both approaches for assessing shielding at a sample site yielded very similar results, giving confidence to our Google Earth approach. Field-based shielding measurements were used in age calculations when available.

Sample preparation

Physical and chemical processing of all rock samples was performed at the University College Dublin School of Earth Sciences. Samples were first crushed and sieved, isolating the 850–255 μm size fraction. Samples then underwent a magnetic separation step using a rare-earth magnet, followed by an initial acid cleaning in 2 L bottles using 6 N HCl and then a mixture of ~5% HF and ~8% HNO_3 within heated ultrasonic tanks for ~12 h. Quartz was then separated from other remaining minerals using lithium polytungstate (LST) density separation. Samples underwent a series of 8 h, then 12 h, then 24 h of acid etches in 2 L bottles within heated ultrasonic tanks using a solution of 1% HF/and 1% HNO_3 to remove potential contamination from meteoric Be and dissolve remaining non-quartz minerals. Sample purity was visually assessed using a binocular microscope before sample dissolution and beryllium extraction chemistry, with additional 24-h etches used for samples that appeared to contain non-quartz material.

Beryllium extraction (UCD)

All samples were processed for ^{10}Be analysis at the UCD cosmogenic isotope facility (UCIF) using a methodology modified from laboratories at the University of Vermont (Corbett et al., 2016) and the University at Buffalo (Kelley et al., 2012). All samples received ~0.25 mg of a low-background ^{9}Be carrier produced by B. Goehring at Tulane

Table 1. Sample information.

Sample name	Material type	Latitude (°N)	Longitude (°E)	Elevation (m a.s.l.)	Thickness (cm)	Shielding
Glen Derry						
GD-21-01	Boulder	57.079167	−3.611041	692	2	0.985*
GD-21-02	Boulder	57.079202	−3.611239	692	3	0.981*
GD-21-05	Boulder	57.078509	−3.618064	730	2	0.974*
GD-21-06	Boulder	57.079234	−3.617830	734	2	0.980*
DD-21-02	Boulder	57.040532	−3.581482	501	2	0.980
DD-21-03	Boulder	57.040047	−3.581966	501	2	0.980
DD-21-04	Boulder	57.039118	−3.585646	516	2	0.980
DD-21-05	Boulder	57.041256	−3.581929	507	2	0.980
Lochain Uaine						
LU-21-01	Boulder	57.062770	−3.645045	957	4	0.987
LU-21-02	Boulder	57.063238	−3.645148	964	1	0.991*
LU-21-03	Boulder	57.064787	−3.645065	990	3	0.995
LU-21-07	Boulder	57.063534	−3.643883	970	2	0.992
Cairngorm Plateau						
CR-21-01	Tor plinth	57.107817	−3.637582	1081	2	1.000
CR-21-02	Bedrock	57.108094	−3.637758	1081	3	1.000
CR-21-04	Perched boulder	57.110869	−3.650713	1080	2	0.998
CR-21-05	Perched boulder	57.110770	−3.650780	1080	3	0.998
CR-21-08	Bedrock	57.112911	−3.651646	1108	1	1.000
FB-21-01	Bedrock	57.096056	−3.661850	1112	1	1.000
FB-21-03	Quartz vein	57.098094	−3.663524	1143	3	1.000
FB-21-04	Bedrock	57.098405	−3.663362	1144	2	1.000

*Samples where shielding was estimated using the Google Earth tool.

University from a deeply mined phenacite crystal that yields long-term $^{10}Be/^{9}Be$ ratios of $1.73 \pm 1.84 \times 10^{-15}$ (Goehring et al., 2021), with Be isolated using ion exchange chromatography. $^{10}Be/^{9}Be$ ratios were measured at the Lawrence Livermore National Laboratory Center for Accelerator Mass Spectrometry. Process blank values ranged from 1.57×10^{-15} to 3.54×10^{-15}, with an average of 2.22×10^{-15} and a standard deviation of 5.61×10^{-16} ($n = 10$), where blank correction was made for each batch of samples processed based on the average concentration of blanks within a batch; see Table 2 for process blank details.

In situ ^{14}C extraction (Purdue)

Purified quartz separates from 11 samples were sent to the Purdue Rare Isotope Measurement Laboratory (PRIME Lab) for *in situ* ^{14}C extraction and measurement using automated procedures (Lifton et al., 2023). Approximately 5 g of quartz from each sample was added to a degassed $LiBO_2$ flux in a reusable 90% Pt/10% Rh sample boat and heated to 500°C for 1 h in ca. 6.7 kPa of Research Purity O_2 to remove atmospheric contaminants, which were discarded. The sample was then heated to 1100°C for 3 h to dissolve the quartz and release the *in situ* ^{14}C, again in an atmosphere of ca. 6.7 kPa of Research Purity O_2 to oxidize any evolved carbon species to CO_2. The CO_2 from the 1100°C step was then collected, purified, measured quantitatively, diluted to ca. 300 μg C-equivalent with ^{14}C-free CO_2, and converted to graphite for ^{14}C AMS measurement at PRIME Lab (Lifton et al., 2023). Measured concentrations of *in situ* ^{14}C are calculated from the measured isotope ratios via AMS following Hippe and Lifton (2014). Due to a procedural irregularity in the first run of FB-21-03, extraction was replicated on another sample aliquot/as a check on the initial result. Both results agreed within 1σ analytical uncertainty (Table 3). The mean and standard deviation are used to correct measured 14C sample inventories; see Table 3 for details.

Analysis/age calculation

Exposure ages were calculated using version 3 of the University of Washington online exposure-age calculator (https://hess.ess.washington.edu/math/v3/v3_cal_in.html) using the CRONUS-Earth global production rate calibration dataset as published in Borchers et al. (2016). for ^{10}Be. The CRONUS-Earth global production rate dataset for *in situ* ^{14}C (Borchers et al., 2016) was augmented by adding all measurements from Young et al. (2014) after recalculating all data per Hippe and Lifton (2014). Please see Koester and Lifton (2023, corrigendum in 2024) for a complete description of the production rate calibration dataset. All production rates were calculated using the LSDn scaling scheme (Lifton et al., 2014; Lifton, 2016). The 'global' production rate was utilized to enable direct comparison between ^{10}Be and ^{14}C production rates calibrated in quartz over a broad range of geologic settings. No correction was applied to these samples for snow cover, as sampled surfaces are believed to be unlikely to accumulate snow due to locally strong wind conditions. Additionally, we do not correct surface erosion, as the amount of erosion estimated since the Lateglacial has a negligible effect on post-LGM exposure ages. We note that the lack of an erosion correction could mean that the amount of exposure that occurred prior to the Last Glacial period may be underestimated here, though pre-LGM landscape evolution is not the focus of this work, thus we choose not to attempt to quantify pre-LGM erosion rates as we feel it would unnecessarily add uncertainty. Finally, no correction is made for postglacial isostatic uplift following arguments made by Young et al. (2020).

Isotopic modeling of ^{14}C and ^{10}Be

We use a MATLAB numerical model of ^{10}Be and ^{14}C cosmogenic nuclide production under variable ice thickness (modified from Pendleton et al., 2019a, 2019b) to explore various ice cover scenarios at sample locations. We note that this code is not publicly posted at present but can be made available on request. Nucleon spallation production under ice-free conditions at each

Table 2. ^{10}Be data.

Sample name	Qtz (g)	^{9}Be (mg)	$^{10}Be/^{9}Be$ ratio ± error (10^{-13})	[^{10}Be] ± error (10^{4} atoms g^{-1})	Age ± 1σ (ka)
Glen Derry					
GD-21-01†	34.612	0.23218	2.1672 ± 0.0405	8.78 ± 0.16	10.7 ± 0.2
GD-21-02†	34.770	0.23195	2.4267 ± 0.0454	9.78 ± 0.18	12.0 ± 0.2
GD-21-05†	35.136	0.23233	2.3788 ± 0.0445	9.5 ± 0.18	11.3 ± 0.2
GD-21-06†	35.216	0.23196	2.3553 ± 0.0440	9.37 ± 0.18	11.0 ± 0.2
DD-21-02‡	18.072	0.23253	1.4737 ± 0.0277	11.454 ± 0.215	16.7 ± 0.3
DD-21-03‡	20.414	0.23124	0.9810 ± 0.0221	6.713 ± 0.151	9.8 ± 0.2
DD-21-04‡	20.419	0.23258	1.5580 ± 0.0381	10.719 ± 0.262	15.3 ± 0.4
DD-21-05‡	19.978	0.23245	1.5208 ± 0.0285	10.689 ± 0.200	15.4 ± 0.3
Lochain Uaine					
LU-21-01†	29.113	0.23194	2.9802 ± 0.0554	14.342 ± 0.267	14.0 ± 0.3
LU-21-02†	34.869	0.23152	3.0904 ± 0.0574	12.395 ± 0.230	11.7 ± 0.2
LU-21-03†	28.728	0.23269	5.3288 ± 0.0987	26.072 ± 0.483	24.3 ± 0.5
LU-21-07†	35.014	0.23223	5.2515 ± 0.0977	21.040 ± 0.391	19.9 ± 0.4
Cairngorm Plateau					
CR-21-01*	15.441	0.30887	3.5573 ± 0.0664	42.983 ± 0.802	36.6 ± 0.7
CR-21-02*	15.034	0.21157	4.6912 ± 0.0873	39.880 ± 0.742	34.2 ± 0.6
CR-21-04*	15.203	0.23209	3.3239 ± 0.0620	30.651 ± 0.572	26.1 ± 0.5
CR-21-05*	15.512	0.23202	2.2417 ± 0.0444	20.254 ± 0.401	17.5 ± 0.3
CR-21-08*	15.026	0.23225	2.6451 ± 0.0494	24.696 ± 0.461	20.3 ± 0.4
FB-21-01*	15.282	0.23263	3.1851 ± 0.0638	29.287 ± 0.586	24.0 ± 0.5
FB-21-03*	15.279	0.23226	3.0817 ± 0.0574	28.29 ± 0.527	23.0 ± 0.4
FB-21-04*	15.268	0.23266	3.0981 ± 0.0527	28.517 ± 0.485	22.9 ± 0.4

^{9}Be carrier concentration (Tulane low level): 904 ppm. All samples measured with 07KNSTD standard at LLNL.
*Associated process blank $^{10}Be/^{9}Be$ ratios (10^{15}): 1.5704 ± 0.2742, 1.910 ± 0.2773, 2.2757 ± 0.3434, 2.3051 ± 0.2680.
†Associated process blank $^{10}Be/^{9}Be$ ratios (10^{15}): 3.5411 ± 0.3184, 2.1039 ± 0.2521, 2.4407 ± 0.2745, 2.4456 ± 0.4392.
‡Associated process blank $^{10}Be/^{9}Be$ ratios (10^{15}): 1.98531 ± 0.3146, 1.5960 ± 0.2259.

Table 3. ^{14}C data.

SAMPLE	PCEGS[a] #	PLID[b]	Mass Quartz (g)	C yield (ug)	Diluted Mass C (ug)	AMS Split Mass C[c] (ug)	$\delta^{13}C$ (‰ VPDB)	$^{14}C/^{13}C$ (10^{-12})	$^{14}C/C_{total}$[d] (10^{-14})	^{14}C[e] (10^6 at)	[^{14}C] (10^5 at g^{-1})	Age ± 1σ (ka)
Cairngorm Plateau												
CR-21-01	PCEGS-181	202301085	5.02409	4.8 ± 0.1	301.3 ± 3.7	292.5 ± 3.6	−45.4 ± 0.2	9.8107 ± 0.2271	10.1470 ± 0.2389	1.4595 ± 0.0434	2.9049 ± 0.0864	15.0 ± 1.3
CR-21-02	PCEGS-183	202301086	5.01690	3.9 ± 0.1	301.9 ± 3.7	293.1 ± 3.6	−45.7 ± 0.2	9.6086 ± 0.2042	9.9322 ± 0.2148	1.4299 ± 0.0403	2.8502 ± 0.0804	14.6 ± 1.1
CR-21-04	PCEGS-184	202301087	5.02658	3.1 ± 0.1	305.8 ± 3.7	296.8 ± 3.6	−46.0 ± 0.2	9.3590 ± 0.1992	9.6673 ± 0.2095	1.4087 ± 0.0398	2.8026 ± 0.0791	13.8 ± 1.0
CR-21-05	PCEGS-186	202301088	5.02804	2.6 ± 0.1	300.3 ± 3.7	291.5 ± 3.5	−45.9 ± 0.2	9.3025 ± 0.1995	9.6080 ± 0.2099	1.3731 ± 0.0393	2.7310 ± 0.0782	13.2 ± 0.9
CR-21-08	PCEGS-188	202301089	5.04029	3.9 ± 0.1	300.6 ± 3.7	291.7 ± 3.6	−45.8 ± 0.2	10.2529 ± 0.2357	10.6090 ± 0.2479	1.5254 ± 0.0449	3.0265 ± 0.0890	15.7 ± 1.4
FB-21-01	PCEGS-189	202301090	5.03058	2.9 ± 0.1	302.8 ± 3.7	293.9 ± 3.6	−45.4 ± 0.2	9.4066 ± 0.2201	9.7231 ± 0.2316	1.4027 ± 0.0423	2.7883 ± 0.0841	12.5 ± 0.9
FB-21-03	PCEGS-191	202301091	5.04343	6.9 ± 0.1	300.9 ± 3.7	292.1 ± 3.6	−45.0 ± 0.2	12.0452 ± 0.2517	12.5040 ± 0.2649	1.8130 ± 0.0486	3.5947 ± 0.0964	Saturated
FB-21-03 R	PCEGS-192	202301092	5.01782	7.7 ± 0.1	303.6 ± 3.7	294.7 ± 3.6	−44.5 ± 0.2	11.6179 ± 0.2513	12.0610 ± 0.2647	1.7624 ± 0.0485	3.5123 ± 0.0967	Saturated
										Mean ± 1σ (FB-21-03)	3.5535 ± 0.0583	Saturated
FB-21-04	PCEGS-194	202301093	5.03119	6.7 ± 0.1	301.1 ± 3.7	292.2 ± 3.6	−44.6 ± 0.2	11.8826 ± 0.2753	12.3370 ± 0.2899	1.7890 ± 0.0517	3.5559 ± 0.1027	Saturated
Lochain Uaine												
LU-21-02	PCEGS-197	202301094	5.04073	4.3 ± 0.1	307.4 ± 3.7	298.4 ± 3.6	−44.9 ± 0.2	8.0800 ± 0.1771	8.3323 ± 0.1864	1.2107 ± 0.0360	2.4019 ± 0.0714	11.9 ± 0.8
LU-21-03	PCEGS-199[f]	202301095	5.03735	4.0 ± 0.1	301.9 ± 3.7	293.0 ± 3.6	−45.8 ± 0.2	8.8064 ± 0.2138	9.0872 ± 0.2249	1.3020 ± 0.0409	2.5847 ± 0.0812	13.8 ± 1.1
LU-21-07	PCEGS-201[f]	202301096	5.01260	3.4 ± 0.1	301.6 ± 3.7	292.8 ± 3.6	−45.7 ± 0.2	8.7635 ± 0.2037	9.0430 ± 0.2142	1.2940 ± 0.0395	2.5814 ± 0.0788	14.2 ± 1.2
Procedural blanks										^{14}C (10^4 at)		
PB1-040423	PCEGS-175	202301102	—	3.5 ± 0.1	314.3 ± 3.8	305.1 ± 3.7	−41.9 ± 0.2	0.7027 ± 0.0538	0.5710 ± 0.0571	8.9987 ± 0.9058	—	—
PB1-041423	PCEGS-178	202301104	—	4.8 ± 0.1	302.5 ± 3.7	293.6 ± 3.6	−46.6 ± 0.2	0.6040 ± 0.0544	0.4622 ± 0.0574	7.0098 ± 0.8740	—	—
PB1-041823	PCEGS-179	202301105	—	2.1 ± 0.1	303.1 ± 3.7	294.2 ± 3.6	-46.4 ± 0.2	0.5909 ± 0.0478	0.4485 ± 0.0505	6.8166 ± 0.7717	—	—
PB1-051323	PCEGS-196	202301107	—	2.4 ± 0.1	301.2 ± 3.7	292.4 ± 3.6	−43.3 ± 0.2	0.7079 ± 0.0523	0.5737 ± 0.0554	8.6643 ± 0.8430	—	—
PB1-060823	PCEGS-208[f]	202301113	—	2.1 ± 0.1	303.1 ± 3.7	294.2 ± 3.6	−46.4 ± 0.2	0.4942 ± 0.0514	0.3470 ± 0.0543	5.2727 ± 0.8274	—	—
									Mean ± 1σ	7.3524 ± 1.5134		

[a]Purdue carbon extraction and graphitization system.
[b]Prime Lab ID.
[c]Mass graphitized for AMS analysis after small aliquot (ca. 9 ug C) taken for stable C isotopic analysis offline.
[d]Corrected for mass-dependent graphitzation blank and stable C composition.
[e]Value corrected for mean procedural blank.
[f]New bottle $LiBO_2$.

sample location was first determined with version 3 of the University of Washington online exposure-age calculator (https://hess.ess.washington.edu/math/v3/v3_cal_in.html) using the same ^{10}Be and ^{14}C production rates in the preceeding section. Spallation production at the sample surface during times of ice cover (i.e., at the rock-ice interface) was determined by applying an attenuation length of 160 g cm^{-2} to the derived ice surface production rates (Gosse and Phillips, 2001).

Muogenic production (considering both fast- and slow-negative muons) for ^{10}Be and ^{14}C under ice was calculated following Balco (2017), with all relevant parameters adjusted for ice. These spallogenic and muogenic production rates, accounting for any imposed ice cover, were combined into a total production rate (P_o) at each timestep of the model. Nuclide concentrations at the sample surface (N) under different ice cover histories were calculated iteratively at time steps (dt) using the following equation:

$$N = [N_o * e^{-\lambda dt}] + \left[\frac{P_o}{\lambda} * (1 - e^{-\lambda dt})\right]$$

where N_o is the existing *in situ* nuclide concentration (at g^{-1}) at the beginning of each timestep, and λ is the respective nuclide decay constant (year^{-1}). In our simulations, rock erosion is assumed to be zero.

Results

Timing of local deglaciation

Twenty samples were collected from five field areas for this study, two of which are basins located on the high plateau between Cairngorm and Ben MacDui (Coire Raibeirt and Fèith Buidhe), one is located within a corrie on the western flank of the Ben MacDui massif (Lochain Uaine), one at the head of Glen Derry, and one lower in Glen Derry at the Derry Dam (Table 1). Of the 20 samples analyzed, all were processed for ^{10}Be (Table 2), while 11 were measured for *in situ* ^{14}C (Table 3). In total, the samples constrain deglaciation from the LGM to the earliest Holocene.

Plateau samples

Eight samples were collected from perched boulders and prominent bedrock outcrops on the Cairngorm plateau; all samples were analyzed for ^{10}Be and ^{14}C. Sampling focused on two south-facing basins in the plateau, Fèith Buidhe and Corrie Raibeirt, both located west of the summit of Cairn Gorm. In Fèith Buidhe, three samples were collected from prominent bedrock outcrops along a ridge forming the basin's eastern margin (Fig. 3). The lowest elevation sample was at 1116 m a.s.l. yielded ages of 24.0 ± 0.5 ka (^{10}Be; FB-21-01) and 12.5 ± 0.9 ka (^{14}C; FB-21-01). Two samples, one from a quartz vein (FB-21-03) in bedrock and another from bedrock (FB-21-04), both located near the highest point on the ridge at ~1140 m a.s.l., yielded similar ^{10}Be ages of 23.0 ± 0.4 ka (FB-21-03) and 22.9 ± 0.4 ka (FB-21-04). ^{14}C concentrations from both samples were at secular equilibrium between production and decay, typically indicative of >25 ky of continuous exposure.

In Coire Raibeirt, five samples were collected from bedrock and perched boulders on the basin headwall and eastern margin (Fig. 4). Ages from ^{10}Be concentrations ranged from 36.6 ± 0.7 ka to 17.5 ± 0.3 ka (Table 2). In contrast, *in situ* ^{14}C concentrations yielded Lateglacial ages between 15.7 ± 1.4 ka and 13.2 ± 0.9 ka, with all samples overlapping at one-sigma

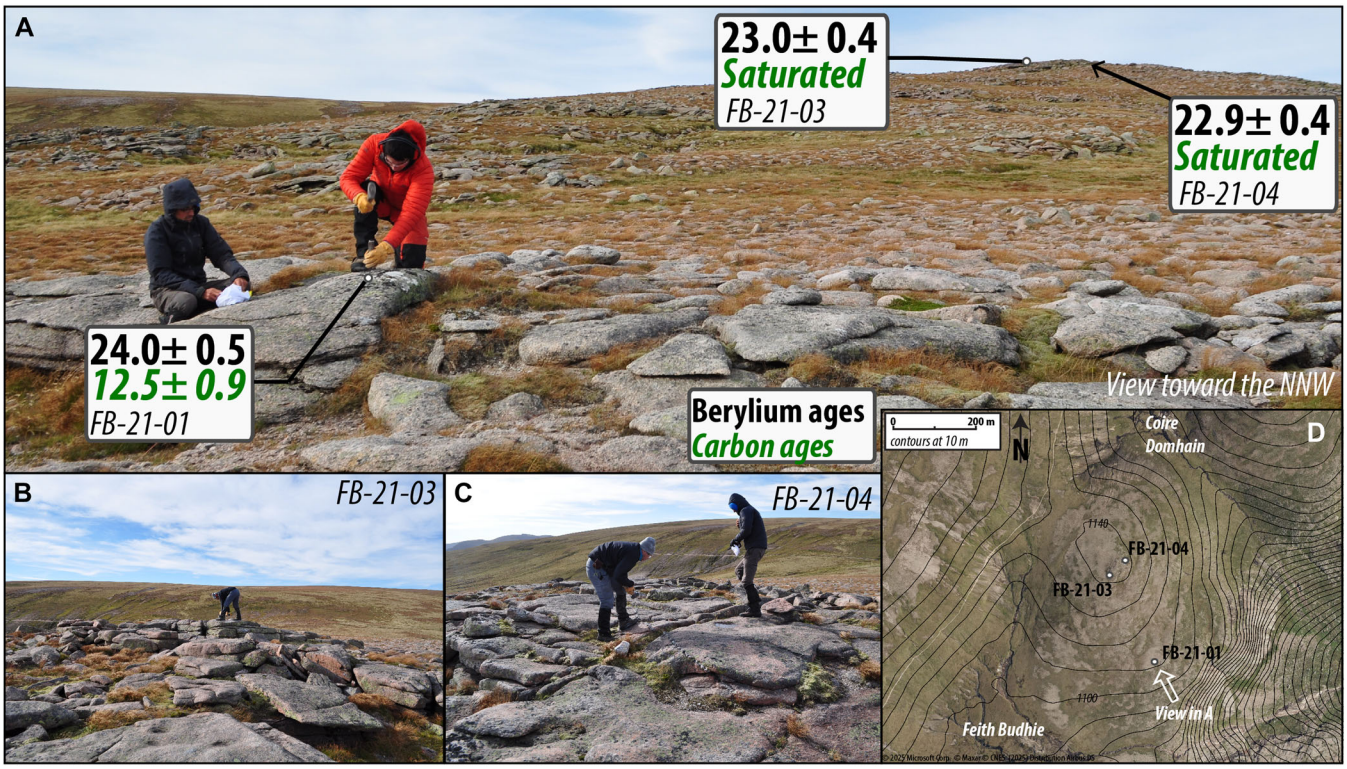

Figure 3. (A) Photograph to the NNE showing the eastern margin of Fèith Buidhe on the Cairngorm Plateau. Sample locations are shown with corresponding exposure ages. The distance between FB-21-01 and FB-21-03 is ~250 m. (B) Photograph of sample site for FB-21-03, view toward the north. (C) Photograph of sample site for FB-21-04, view toward the NW. (D) Satellite image with 10 m topographic contours showing the sampling area and sample locations. Contours generated from 5 m DTM (Landmap, 2014) and satellite image from Vexcel satellite imagery downloaded from Bing Aerial Imagery (Microsoft, 2025). [Color figure can be viewed at wileyonlinelibrary.com]

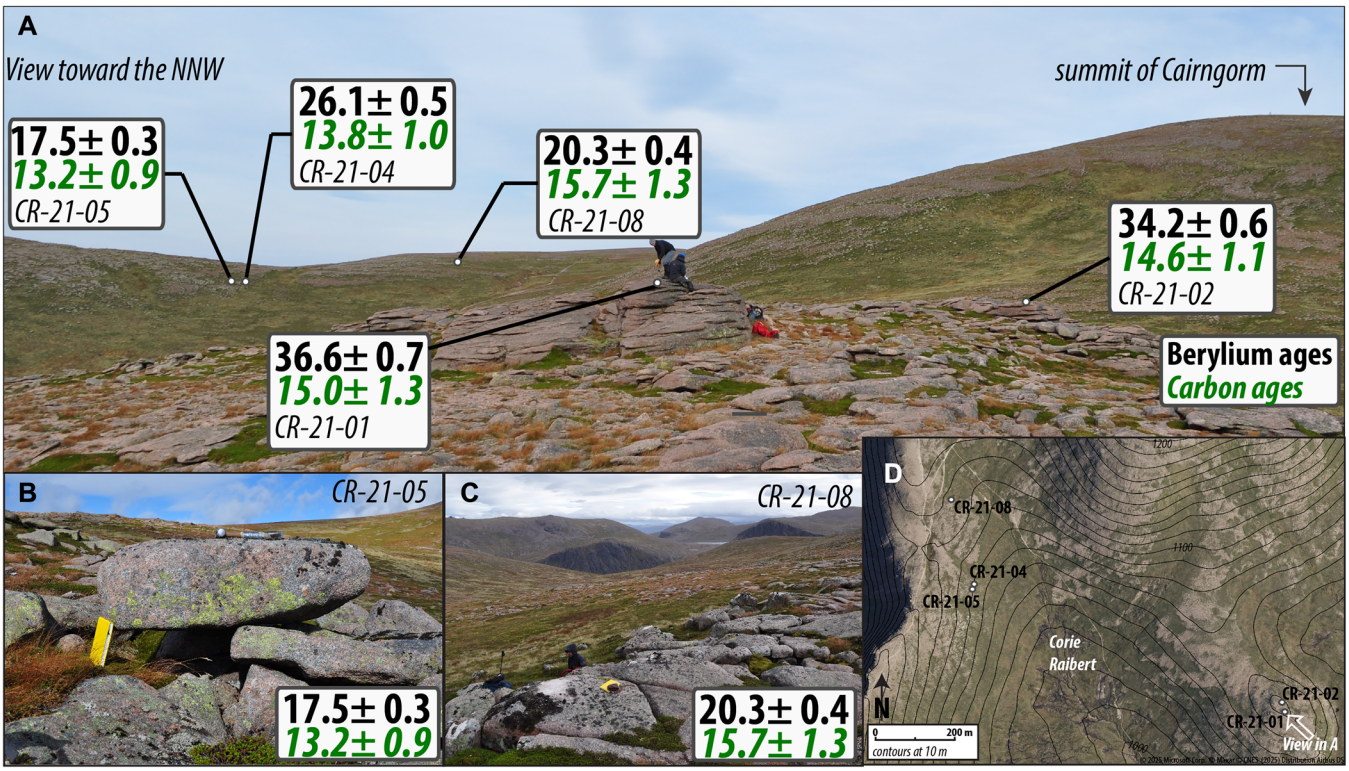

Figure 4. (A) Photograph to the NNW across Coire Raibeirt. Sample locations are shown with corresponding exposure ages. The distance between samples in the foreground and CR-21-08 is ~1 km. (B) Photograph of sample site for CR-21-05, view toward the NE. (C) Photograph of sample site for CR-21-08, view toward the SE. (D) Satellite image with 10 m topographic contours showing the sampling area and sample locations. Contours generated from 5 m DTM (Landmap, 2014) and satellite image from Vexcel satellite imagery downloaded from Bing Aerial Imagery (Microsoft, 2025). [Color figure can be viewed at wileyonlinelibrary.com]

uncertainty, yielding a mean age and standard error of 14.5 ± 0.4 ka (Table 3).

Lochain Uaine

Within the Lochain Uaine corrie, elevation of ~960 m a.s.l., samples from four boulders were collected from two prominent moraines (Fig. 5). Two samples from the outer moraine yielded ^{10}Be ages of 24.3 ± 0.5 ka (LU-21-03) and 19.9 ± 0.4 ka (LU-21-07), while *in situ* ^{14}C ages were younger, 13.8 ± 1.1 ka (LU-21-03) and 14.2 ± 1.2 ka (LU-21-07), overlapping at one-sigma uncertainty. The inner moraine yielded younger ages for both nuclides, with one sample analyzed for both ^{10}Be and ^{14}C yielding overlapping ages of 11.7 ± 0.2 ka (^{10}Be; LU-21-02) and 11.9 ± 0.8 ka (^{14}C; LU-21-02). A second sample from the same moraine yielded a ^{10}Be age of 14.0 ± 0.3 ka (LU-21-01).

Glen Derry samples

Four samples were collected from boulders embedded in a broad moraine complex which crosses the southern terminus of Glen Derry, known as the Derry Dam, at 500 m a.s.l.; these samples were analyzed for ^{10}Be. (Fig. 6). Two samples from the ice proximal crest of the moraine yield statistically identical ages of 15.3 ± 0.4 ka (DD-21-04) and 15.4 ± 0.3 ka (DD-21-05), while two samples from the distal slope yield ages of 16.7 ± 0.3 ka (DD-21-02) and 9.8 ± 0.2 ka (DD-21-03).

Approximately 5 km up the valley, two samples were collected from boulders embedded in the most ice-proximal (westerly) of a series of recessional moraines (Fig. 7). The two ^{10}Be ages, from boulders located ~25 m apart, at an elevation of 690 m a.s.l. are 10.7 ± 0.2 ka (GD-21-01) and 12.0 ± 0.2 ka (GD-21-02). The discrepancy in these ages may result from inherited nuclides in the older sample or postdepositional modification of the younger sample. Given the chronology up and down valley from this site, we favor the older age as the likely timing of deglaciation. Finally, two samples from boulders were collected from the most up-valley moraine in the valley system, located 400 m west of GD-21-01 and -02. Ages from the two samples overlapped within uncertainty and were 11.3 ± 0.2 ka (GD-21-05) and 11.0 ± 0.2 ka (GD-21-06).

Discussion

Spatiotemporal pattern of ice recession: LGM thinning

The earliest evidence of ice-free conditions in our Cairngorm chronology comes from our highest elevation samples at ~1140 m a.s.l., where two samples from a local topographic high indicate local deglaciation occurring during the LGM. The two samples, FB-21-03 and FB-21-04, contain *in situ* ^{14}C concentrations at a secular equilibrium between production and decay (colloquially referred to as 'saturated'). Typically, a saturated concentration represents >25 ky of continuous exposure. ^{10}Be concentrations from the same samples indicate overlapping exposure ages of 23.0 ± 0.4 and 22.9 ± 0.4 ka. Given the concentrations and modeled ages for the two isotopes, the simplest explanation for these nuclide concentrations is a single period of continuous exposure initiating at ~23 ka. Notably, our ^{10}Be ages fall within the error of both ^{10}Be and ^{26}Al ages from a tor at 1230 m a.s.l. located on the eastern flank of the summit of Cairn Gorm 2 km to the northeast (Fig. 2(A)), which yielded ages of 23.4 ± 1.9 ka (^{10}Be); 26.4 ± 11.9 ka (^{26}Al) for sample CG1A and 27.8 ± 3.0 ka (^{10}Be); 26.0 ± 4.2 ka (^{26}Al) for sample CG1B (Phillips et al., 2006). When viewed collectively, these

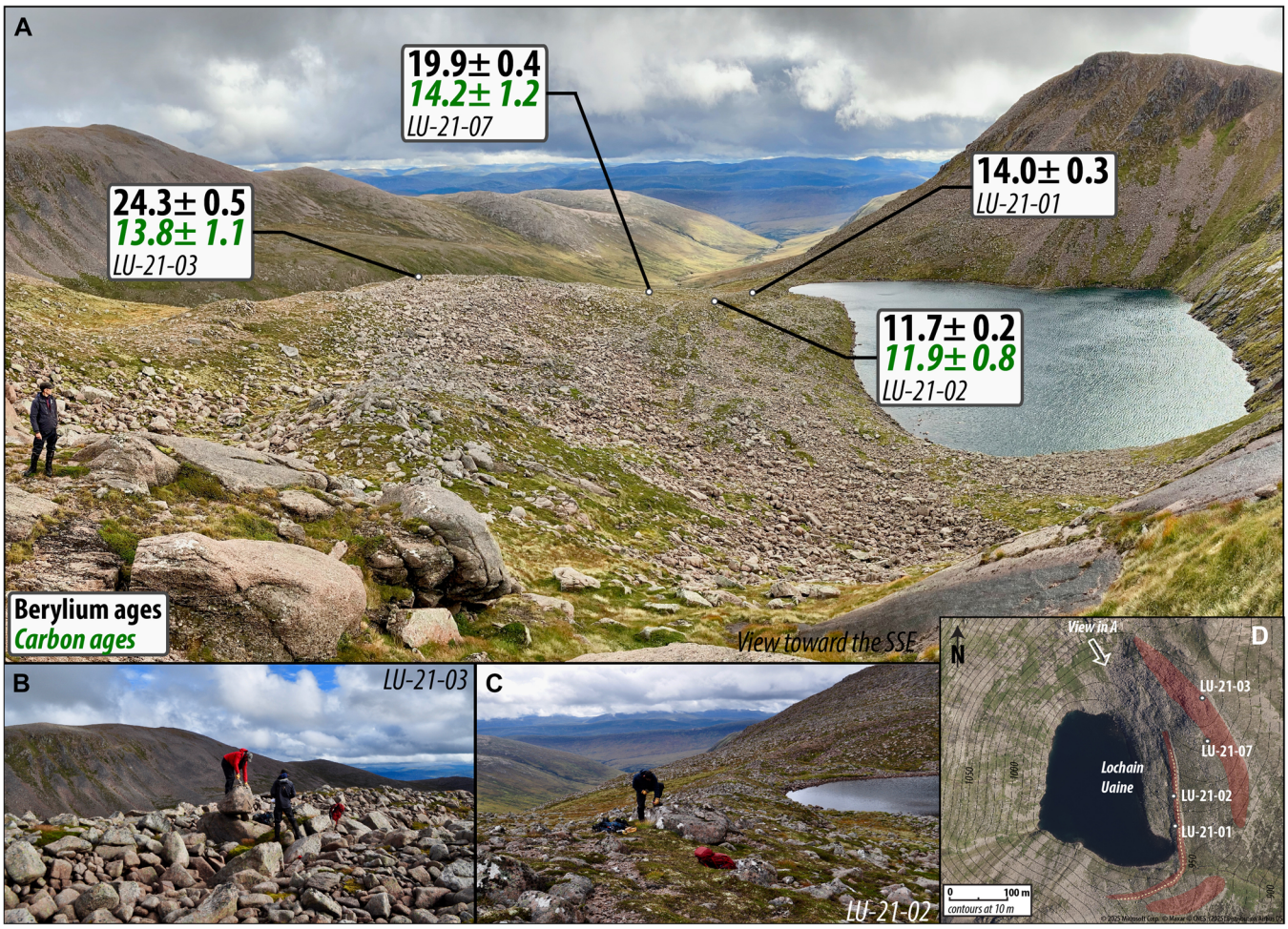

Figure 5. (A) Photograph looking SSE across Lochain Uaine, showing sample locations from inner and outer corrie moraines with corresponding exposure ages. The moraine at Lochain Uaine is shown from the opposite side of the basin in Fig. 2(D). (B) Photograph of sample site for LU-21-03, view toward the SE. (C) Photograph of sample site for LU-21-02, view toward the south. (D) Satellite image with 10 m topographic contours showing the sampling area and sample locations with glacial-geomorphic mapping from Standell (2014). Red-shaded regions are moraines with dotted lines indicating the position of the moraine crest. Contours generated from 5 m DTM (Landmap, 2014) and satellite imagery from Vexcel satellite imagery downloaded from Bing Aerial Imagery (Microsoft, 2025). [Color figure can be viewed at wileyonlinelibrary.com]

exposure ages indicate a period of thinning of the BIIS, exposing these high-elevation surfaces during the LGM. This scenario would require rock surfaces previously shielded by the BIIS to become exposed during the last glacial period and remain exposed until the present.

Our remaining samples from the Cairngorm Plateau, as well as others measured in Phillips et al. (2006), document a significant, although variable, degree of ^{10}Be isotopic inheritance preserved within rock material on the plateau, consistent with cold-based glaciation lacking significant glacial erosion. Hall and Phillips (2006) noted that despite cold-based conditions, toppling of tors and movement of large blocks occur during glacial periods due to enhanced basal creep and entrainment by the ice mass. We assume these processes affected both our highest elevation sample sites at some point during the last glacial period, providing an inheritance-free surface for both ^{10}Be and ^{14}C to begin accumulating due to ice sheet thinning at ~23 000 years ago. Numerical modeling of sample FB-21-04 corroborates this interpretation by showing that both the measured ^{10}Be and ^{14}C concentrations can be achieved with a single period of exposure (Fig. 8).

Exposure of a bedrock surface in central Scotland during the LGM is unexpected, though the presence of nunataks in the BIIS has been theorized many times (e.g., McCarroll et al., 1995; Rae et al., 2004; Hughes et al., 2022), although many mapped trimlines in Britain and Ireland have been reinterpreted as englacial transitions between cold-based ice above and warm-based ice below (e.g., Ballantyne, 2010; Fabel et al., 2012; McCarroll, 2016). Recent reconstructions of the BIIS place the period of maximum ice sheet volume between 24 and 22 ka (Clark et al., 2022), while the Scottish sectors of the BIIS are constrained to positions on the continental shelf in the northeast, confluent with the Scandinavian Ice Sheet to the east (Graham et al., 2007; Sejrup et al., 2016; Bradwell et al., 2021), with retreat occurring within the Minch and in the Malin Sea (Benetti et al., 2021; Bradwell et al., 2021). The same reconstruction places ~1000 m of ice over the collection sites for samples FB-21-03 and FB-21-04 23 000 years ago (Clark et al., 2022), indicating a significant mismatch between the model and local geologic data. Given the large areal extent of the high-elevation Cairngorm Plateau, this mismatch cannot solely be attributed to the coarse spatial grid on which the numerical model is run. We note that other work with cosmogenic nuclides has yielded exposure ages of >20 ka from topographic highs in this part of Scotland (e.g., Phillips et al., 2006; Phillips et al., 2008; Hall et al., 2016; Hall et al., 2024), yet most studies utilize ^{10}Be and/or ^{26}Al, thus are unable to resolve the presence a nunatak from the last glacial period. Only one study, which focuses on Lochnagar, located approximately 30 km southeast, uses paired ^{14}C and ^{10}Be, thus circumventing issues with single nuclide inheritance (Hall et al., 2024).

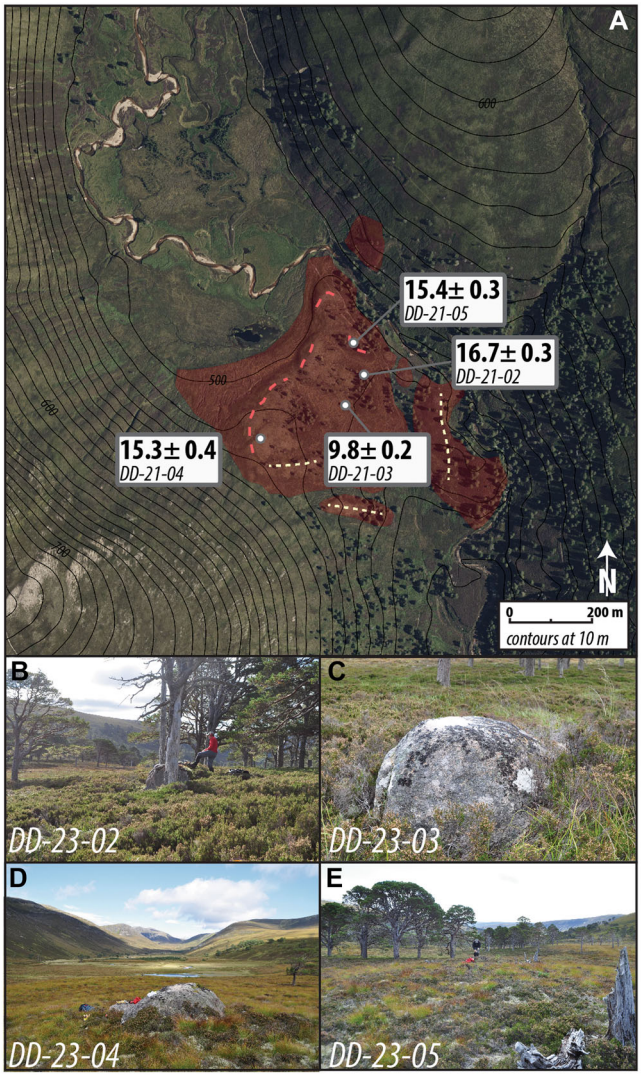

Figure 6. (A) Satellite image with 10 m topographic contours showing the Derry Dam sampling area and sample locations at the southern terminus of Glen Derry with glacial-geomorphic mapping from Standell (2014). Red shaded regions are moraines with dotted lines indicating the position of the moraine crest, yellow lines from the original publication, and red lines added from this study. Panels (B)–(E) show photos of the sampled boulders on the Derry Dam. The points of view in each photo are SE (panel B); W (panel C); NW (panel D); SE (panel E). [Color figure can be viewed at wileyonlinelibrary.com]

Recalculating those ages using the same methods as in this study, the two highest elevation samples analyzed for both ^{14}C and ^{10}Be (LO16-1a and -2a) yield two statistically identical ^{14}C ages of 17.6 ± 1.0 and 16.8 ± 1.0 ka from different levels on the same tor, with ^{10}Be ages indicative of inheritance, 28.3 ± 1.0 and 60.9 ± 2.1 ka, and are thus indicative of cold-based ice cover, with the deglaciation of Lochnagar, ~950 m a.s.l., at ~17 ka. Proxy records of past climate during this period indicate sustained stadial conditions (Svensson et al., 2008), suggesting that the emergence of a Cairngorm nunatak is unlikely to be solely climatically driven. Rather, we theorize that the ice sheet thinning responsible for the exposure of a portion of the high Cairngorm plateau is likely driven by internal BIIS dynamics, with thinning resulting from shifting dispersal centers. The BIIS was undergoing a reorganization between 25–23 ka, with the retreat of northern marine sectors, with ice marginal advance to the south in Cheshire and Yorkshire, as well as across the Dogger Bank and loss of ice mass via the Irish Sea and Malin ice streams (Clark, et al. 2022). This reorganization may have shifted the central dome of the BIIS off the Cairngorm Mountains, yet not Lochnagar (Hall et al., 2024), allowing for the exposure of nunataks over 1100 m a.s.l. Furthermore, it has been proposed that the Cairngorm may have undergone wind-stripping of snow cover and enhanced ice loss via sublimation, analogous to blue ice moraines found in Antarctica (Sugden and Hall, 2020), which could play a role in local ice surface lowering. Regardless the mechanism(s) at play, the existence of an LGM age nunatak within a core region of the BIIS yields implications for the geometry of the BIIS ice surface both locally and further afield, though without further samples from other regional topographic highs, it is difficult to speculate on the extent of the lowered ice surface and thus the effect on ice surface gradient. Further work with paired ^{14}C–^{10}Be exposure dating and numerical modeling is needed to explore this topic further.

Lateglacial exposure of the Cairngorm plateau

Deglaciation of the Cairngorm plateau below 1140 m a.s.l occurred during the later stages of the Lateglacial period. Our samples from below 1140 m a.s.l. on the plateau exhibit discordant ^{10}Be versus ^{14}C ages. Our ^{10}Be ages range from 36.6 ± 0.7 to 17.5 ± 0.3 ka, similar to the findings of Phillips et al. (2006), with variable amounts of nuclide inheritance. In contrast to ^{10}Be results, ages modeled from ^{14}C concentrations yield a much tighter population ranging from 15.7 ± 1.4 to 12.5 ± 0.9 ka, with five ages from the Coire Raibeirt basin consistent at one sigma uncertainty. If we assume our samples experienced a single period of ice cover followed by deglaciation, our ^{14}C ages suggest the last ice receded from this part of the plateau during the Bølling–Allerød. Numerical simulations of the Coire Raibeirt samples under a single exposure scenario concur with deglaciation during the Bølling–Allerød, as well as highlight the variable amounts of inherited ^{10}Be required (Figs. 8 and S1). The ages from samples within Coire Raibeirt may hint at the spatial pattern of deglaciation, with the oldest ^{14}C derived ages in the basin coming from the highest elevation site on the basin's headwall, 1117 m a.s.l., of 15.7 ± 1.4 ka, with similar ages from the eastern margin of the basin at 15.0 ± 1.3 and 14.6 ± 1.1 ka. The youngest ages from Coire Raibeirt come from lower elevation samples on the basin's headwall, both at 1078 m a.s.l., of 13.8 ± 1.0 and 13.2 ± 0.9 ka, perhaps hinting at the shrinking ice mass into Coire Raibeirt during the end of the Allerød interstadial (Fig. 9).

Numerical glacier modeling experiments have speculated about the possibility of glacier growth across much of the Cairngorm Mountains during the Younger Dryas cooling (Golledge et al., 2008; Doughty et al., in review). If glaciers regrew over our sample sites, this would have driven a short-lived period of reduced ^{10}Be and ^{14}C production in our samples due to attenuated production under ice cover and ongoing decay; thus, any period of ice cover during the Younger Dryas would require earlier initial deglaciation. A local chironomid-derived summer temperature record from Abernethy Forest demonstrates warming during the Bølling–Allerød followed by pronounced cooling between 13.1 ka and 11.4 ka (Fig. 9; Brooks et al., 2012). Numerical modeling of Cairngorm ice masses, driven by the Abernethy chironomid record, yields short-lived glacier regrowth of 1200 years between 12.8 ka and 11.6 ka in response to this period of cooling (Doughty et al., in review). Imposing a 1200-year period of ice cover during the Younger Dryas in our isotopic model places the timing of deglaciation ~1500 years earlier, closer to the start of the Bølling–Allerød interstadial for plateau samples collected below 1140 m a.sl. (Figs. 8 and S2). The two primary aspects of the numerical isotope model results that

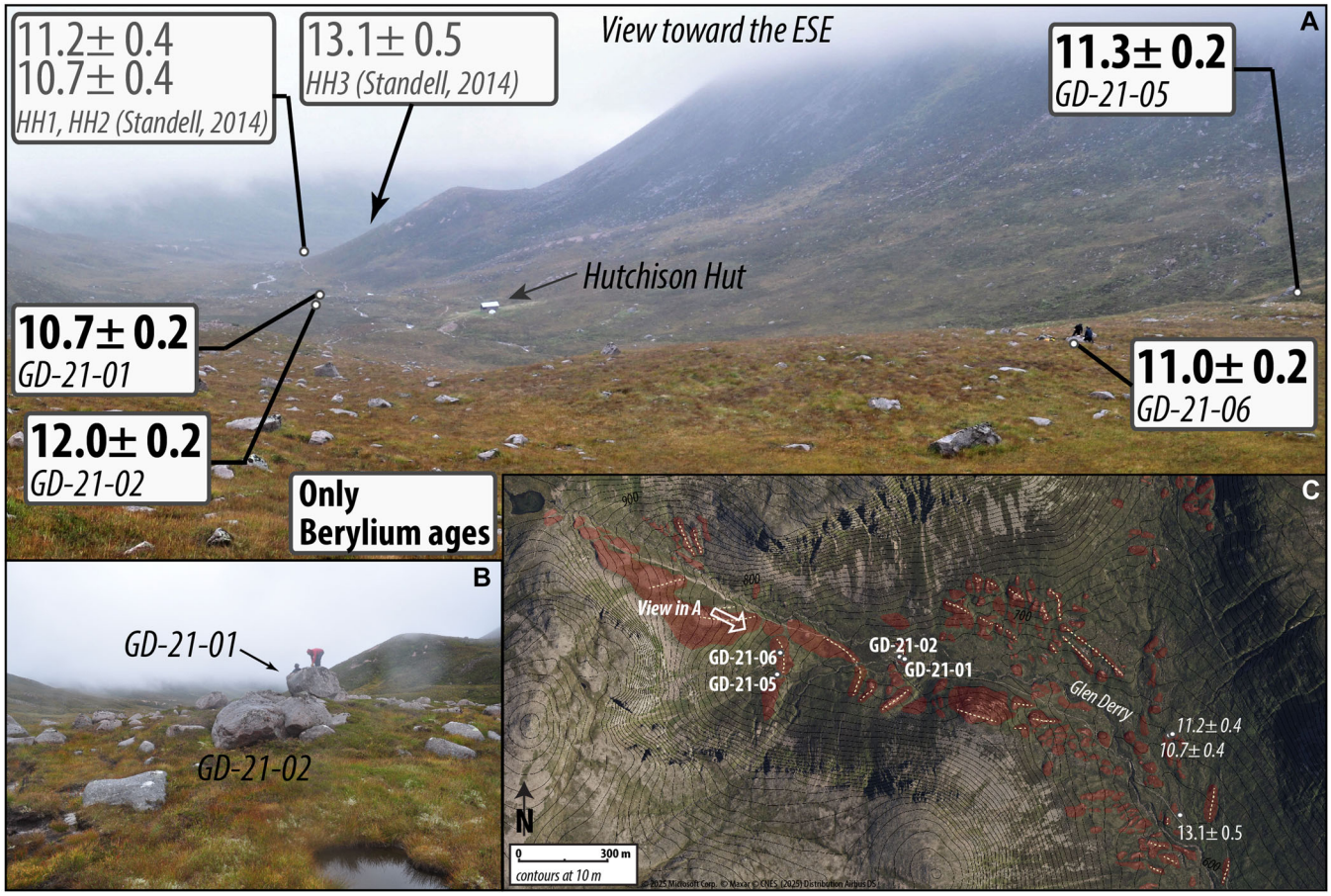

Figure 7. (A) Photograph toward the ESE of upper Glen Derry, showing the location of samples collected with corresponding exposure ages. Also included is the location of samples from Standell (2014). The distance between the samples GD-21-05 and -06 in the foreground and samples GD-21-01 and GD-21-01 is ~400 m. (B) Photograph looking SE toward the boulders sampled for GD-21-01 (background) and GD-21-02 (foreground). (C) Satellite image with 10 m topographic contours showing the sampling area and sample locations with glacial-geomorphic mapping from Standell (2014). Red-shaded regions are moraines with dotted lines indicating the position of the moraine crest. Contours generated from 5 m DTM (Landmap, 2014) and satellite image from Vexcel satellite imagery downloaded from Bing Aerial Imagery (Microsoft, 2025). [Color figure can be viewed at wileyonlinelibrary.com]

add uncertainty to the scenarios are as follows: (1) the thickness of ice during the LGM, theorized to be ~1000 m from Clark et al. (2022), and (2) timing of maximum ice thickness at the LGM. In imposing stepwise, instantaneous, deglaciation from the LGM ice thickness, we see a negligible change in modeled deglaciation age for our samples, which is due to a reduced period of muogenic production leading up to ice-free conditions (Fig. S3). Similarly, imposing only 100 m of ice thickness through the last glacial and the LGM shifts deglaciation ages by only ~100–300 years younger, primarily due to elevated muon production as ice thins during deglaciation (Fig. S4).

Lochain Uaine

Deglaciation of the high corrie, Lochain Uaine, appears to have been interrupted by two readvances or stillstands that formed moraines, one at ~14 ka and then later at ~12 ka. The first moraine building event may have been climatically driven by the short-lived Older Dryas (14.2–13.9 ka) or may have occurred in response to unbuttressing resulting from the removal of ice from the main valley, which would be roughly coincident with the deglaciation of the plateau. The inner moraine is constrained by ^{10}Be and ^{14}C ages from a single sample, where the overlapping ages suggest a single period of exposure starting toward the end of the YD at ~11.8 ka (Fig. 9). Given that the ages result from a single boulder, we cannot rule out postdepositional modification of the sample; thus, we interpret this moraine as from the Pleistocene–Holocene transition and younger than the stratigraphically outboard moraine at ~14 ka.

Glen Derry

In conjunction with three previously published ages from Standell (2014), our chronology constrains the recession of a paleo-glacier up Glen Derry during the Lateglacial into the earliest Holocene. Our oldest ages come from a large terminal moraine, the Derry Dam, near the southern terminus of Glen Derry. Using the oldest two ages from the moraine crest, the glacier system receded from the Derry Dam moraine at 15.3 ± 0.1 ka using the mean and standard error. This timing of moraine formation correlates with ages from boulders on moraines in the Glenmore Basin and Glen Einich on the northern margin of the Cairngorm Mountains, which record fluctuations of Strath Spey and Cairngorm ice masses, respectively. When combined with this dataset, ages on moraine emplacement in the Cairngorm region yield an average age for moraine formation of 15.2 ka and a standard deviation of 900 years (n = 16, one old outlier omitted; Everest and Kubik, 2006; Hall et al., 2016). In western Scotland, the Wester Ross Readvance is correlated to a prominent moraine believed to have been formed by a readvance during retreat of the Scottish Ice Cap (Robinson and Ballantyne, 1979). ^{10}Be ages from boulders from the moraine yield an average age of 15.1 ka and a standard deviation of 1400 years (n = 30; Everest et al., 2006; Bradwell et al., 2008, 2021; Ballantyne et al., 2009b), overlapping with those from the

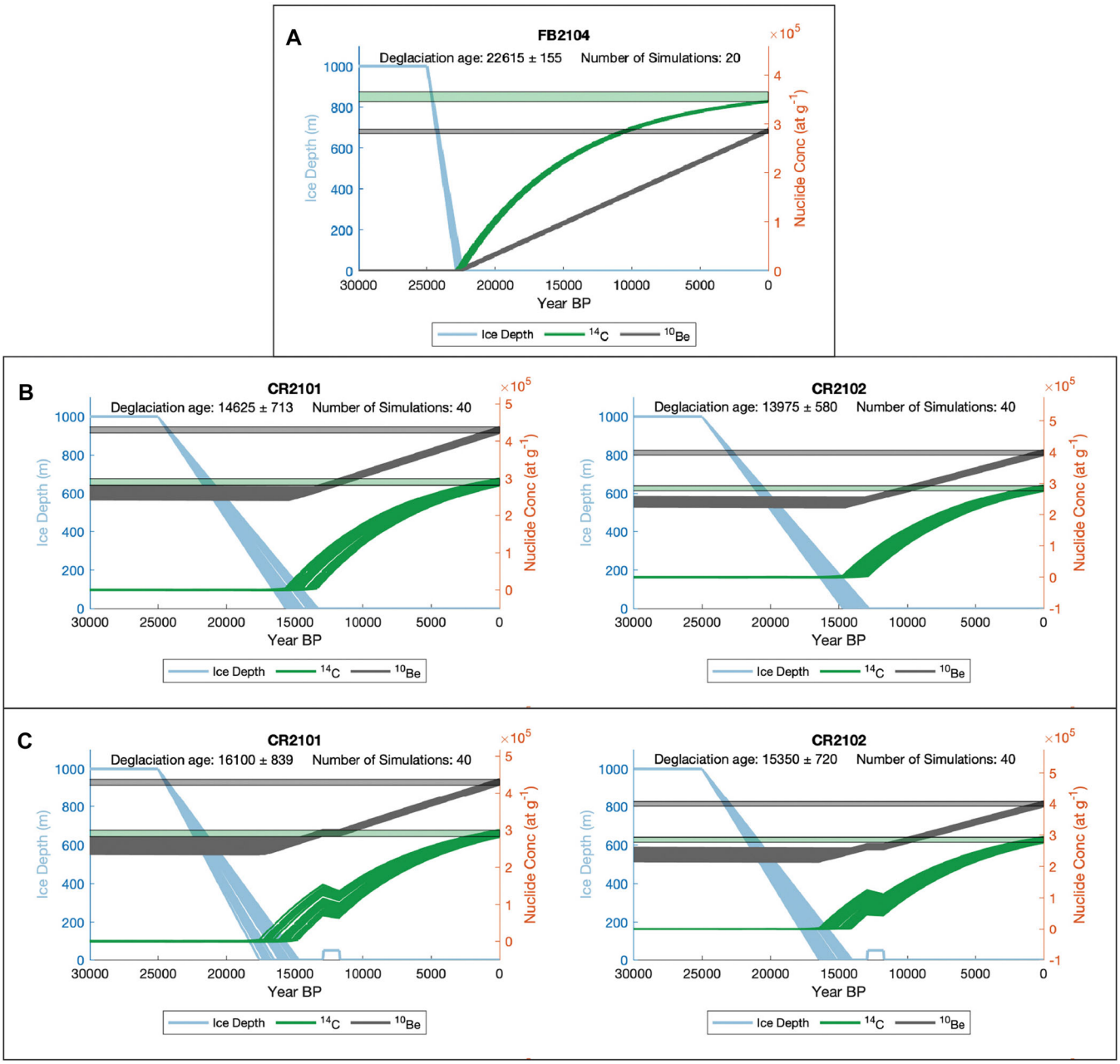

Figure 8. Results of isotopic modeling studies examining possible ice cover scenarios for selected plateau locations. (A) Illustrates the single period of exposure at the highest elevation sample that produces observed ^{10}Be and ^{14}C. (B) Shows the variable timing of deglaciation and inherited ^{10}Be required for two sample locations within Coire Raibeirt for a single period of exposure since deglaciation. (C) Illustrates the impact of an imposed period of ice cover during the Younger Dryas for the same samples as presented in panel B, which necessitates an earlier deglaciation. See Supplement for full model details and results. [Color figure can be viewed at wileyonlinelibrary.com]

Cairngorm region. In total, these 46 ^{10}Be ages from moraines across Scotland provide a record of uniform moraine deposition from independent ice masses, indicative of a single climatic driver (Fig. 10). Lateglacial moraines yielding exposures ages of ~15 ka are not uncommon around the Atlantic Basin, with similar chronologies from moraines in the northeastern United States (Davis et al., 2015; Hall et al., 2017; Koester et al., 2017) and western Europe (Nygård et al., 2004; Clark et al., 2009; Gump et al., 2017; Barth et al., 2018). Previously, the Wester Ross Readvance has been correlated to Greenland Stadial 2a, recorded in Greenlandic ice cores, with the readvance of ice masses driven by cooling in addition to increased precipitation resulting from the decay of surrounding marine-based ice masses (Fig. 10; Hall et al., 2016). Recently updated Mg/Ca sea surface temperature records from the North Atlantic depict cooling just prior to 15 ka, possibly providing evidence for a cooling event that correlates to the timing of Scottish moraine formation (Morley et al., 2024). An alternative hypothesis is that these moraines represent the last ice margin fluctuation recorded in the glacial-geomorphic record before the onset of large-scale recession in response to Bølling–Allerød warming across the Atlantic basin. Additional chronology and high-resolution climatic records are needed to resolve linkages between these moraines and Lateglacial climatic forcing.

Ice margin retreat from Derry Dam progressed up the valley ~4 km to an area of hummocky moraine that fills the valley floor where Glen Derry turns sharply to the west, with a hanging valley that continues northward (Standell, 2014). Three ages from the deposit are in stratigraphic order, with the oldest age (13.1 ± 0.5 ka) located 300 m down valley from two adjacent samples yielding ages of 11.2 ± 0.4 and 10.7 ± 0.4 ka (Standell, 2014). These ages may represent a pause or slowdown in glacier recession between 13 and 11 ka. At the head of the valley, two ages on the uppermost recession moraine in Glen

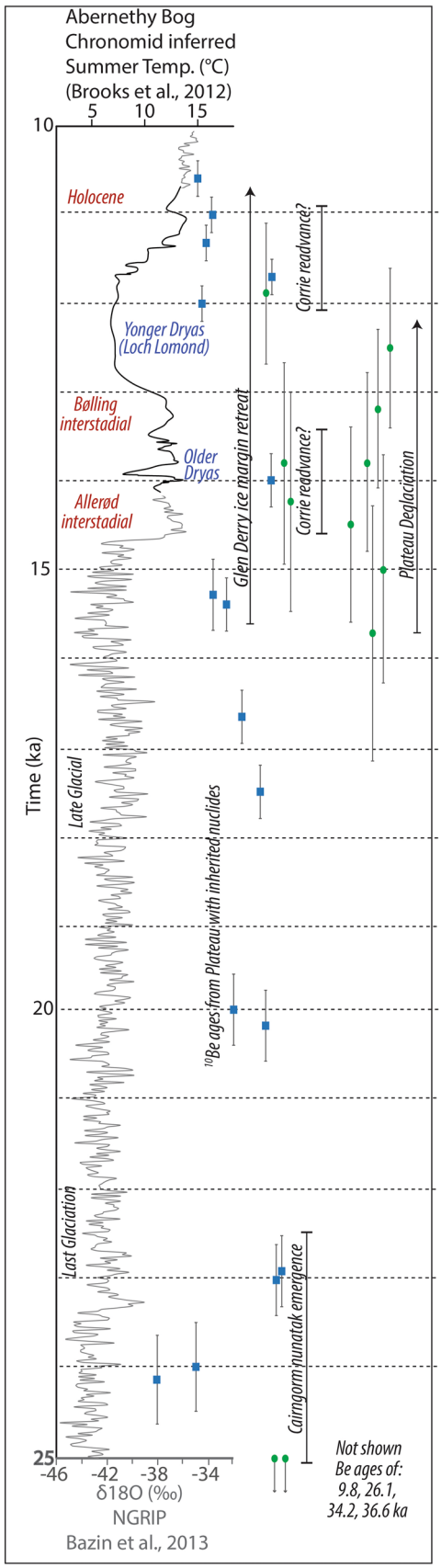

Figure 9. Deglacial chronology produced in this study placed in the context of climatic proxy records from Abernethy Bog, a chironomid summer temperature reconstruction; upper black curve (Brooks et al., 2012), and the North GRIP ice core oxygen isotope record; lower gray curve (Bazin et al., 2013). Interpretation of ice mass change is noted next to the corresponding ages. Blue squares depict ages from ^{10}Be, while green circles represent ages from ^{14}C, with arrows indicating saturated samples. [Color figure can be viewed at wileyonlinelibrary.com]

Derry indicate recession of the valley's upper reaches by 11.1 ka, with rapid retreat 1.5 km up the valley from the hummocky moraine. In total, ice-marginal retreat within Glen Derry covered just under 5.5 km in ~4000 years, or a net retreat rate between 1 and 1.5 m per year, faster if the hummocky moraine deposition resulted from a significant readvance.

Spatial pattern of isotopic inheritance

Our ^{10}Be ages ranged from well before the LGM (36.6 ± 0.7 ka) to Holocene in age (9.7 ± 0.2 ka), while the ^{14}C ages form a tighter cluster, with two samples at secular equilibrium indicative of deglaciation prior to the Lateglacial and the remaining ages between 15.4 ± 1.3 ka and 11.9 ± 0.8 ka. Importantly, there is a clear relationship between sample age and elevation, as previously noted in Britain and Ireland by Ballantyne (2010), where most samples collected below 900–800 m a.s.l. yield ages that appear to have minimal to no inheritance, while samples above 900 m a.s.l. present a wider range of ages. In our dataset, this is exemplified by a marked disagreement between ^{14}C and ^{10}Be above 1000 m a.s.l., indicating the presence of inherited ^{10}Be inventories in the samples (Fig. 11). Samples from the high elevation sites yielded the largest spread in ^{10}Be ages, likely driven by variable quantities of inherited nuclides. This variability in the cosmogenic nuclide concentrations seen across the Cairngorm Mountains, also observed by Phillips et al. (2006), is driven by the net effect of ice cover and landscape modification over multiple glacial cycles. Samples from lower elevations, such as those from Lochain Uaine, yield mixed results, with three samples appearing to contain varying levels of ^{10}Be inheritance compared to ^{14}C ages. In contrast, one sample yields nearly identical ^{14}C and ^{10}Be ages, indicating a lack of inherited ^{10}Be and a simple exposure history. Our highest elevation samples from Glen Derry all yield ages near the Holocene–Pleistocene transition, which is in line with other evidence for the timing of local deglaciation, suggesting that there is little to no inheritance in the glacially transported boulders that were sampled. Furthermore, this indicates that glacially transported boulders in the lower elevation valleys are either: a) sourced from the valley walls that have undergone sustained glacial erosion; or b) boulders sourced from higher in the landscape have undergone sufficient erosion to remove inherited nuclides found on outer surfaces.

When viewed in the context of all ^{10}Be cosmogenic exposure ages from the Cairngorm region (published and those in this study; $n = 104$), a similar, yet less defined pattern emerges with lower elevation samples yielding predominantly Lateglacial and Holocene ages (Fig. 12). A high concentration of post-LGM ages, centered on ~15 ka, exist below 800 m, including samples in our dataset from Derry Dam, while a second cluster of ages exists at 11.4 ka, which includes our samples from upper Glen Derry and Lochain Uaine (Fig. 12), perhaps reflecting a sampling bias favoring post-LGM landforms. Nevertheless, lower elevation samples with relatively high ^{10}Be concentrations exist, emphasizing the spatial variability of cold-based conditions across a topographically complex landscape, as well as the ability of material to travel from a landscape characterized by preservation to one of glacial erosion and transport. This mechanism is illustrated by sample CA-2 from Phillips et al. (2006), yielding a ^{10}Be age >150 ka. Sample CA-2 is from a tor, located at 652 m a.s.l. on An Cnoidh, indicating that the englacial thermal boundary was as much as 350 m lower in the eastern Cairngorm Mountains than in our field area. In contrast, sample DDL-2 is from the side of an erratic boulder at 760 m a.s.l on Da Dhruim Lom, yielding a ^{10}Be age of ~42 ka. The sample exhibits pronounced weathering pits on the sampled surface and was presumably rotated at least once since entrainment and transport,

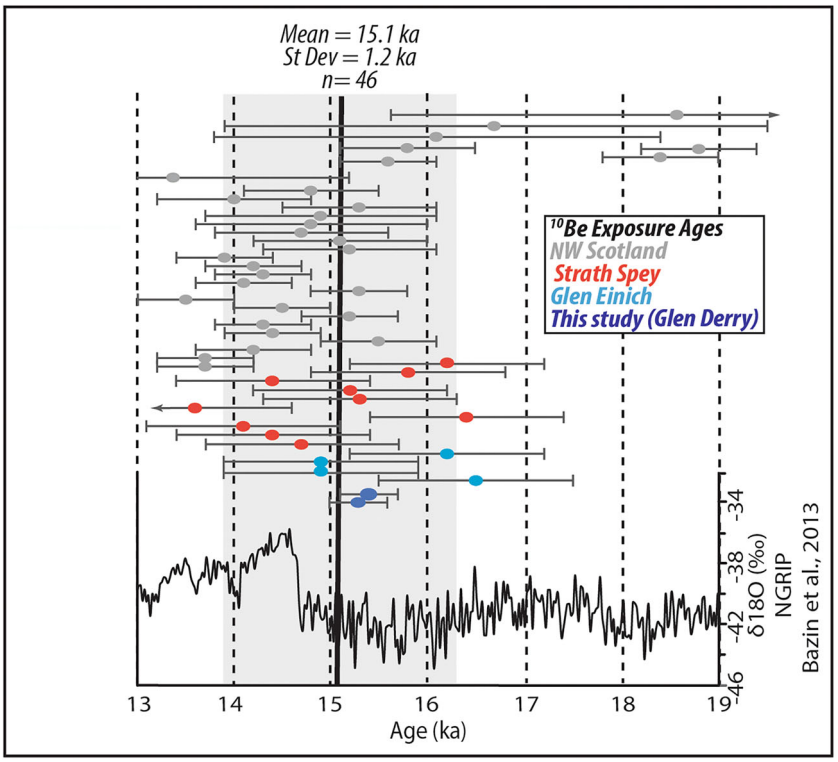

Figure 10. Compilation of ^{10}Be ages derived from boulders on moraines in Scotland during the timing of the Wester Ross Readvance; ages from this study are plotted with those from the Cairngorm and Western Scotland (Everest and Kubik, 2006; Everest et al., 2006; Bradwell et al., 2008; Ballantyne et al., 2009b; Hall et al., 2016; Bradwell et al., 2021). Exposure ages from moraines across Scotland center on 15.1 ka, a relatively cool period, preceding Bølling–Allerød warming. All ages are recalculated using the production rate dataset of Borchers et al. (2016) and LSDn scaling (Lifton et al., 2014; Lifton, 2016). Ages are plotted with the oxygen isotope record of the North GRIP ice core, showing regional climate (Bazin et al., 2013). See Appendix A for a table of sample information. [Color figure can be viewed at wileyonlinelibrary.com]

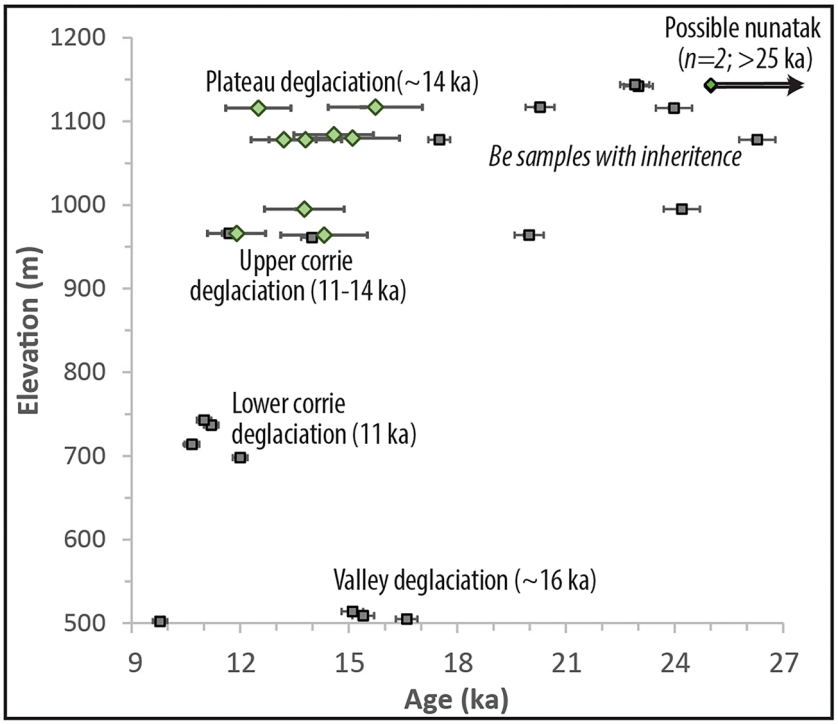

Figure 11. ^{10}Be and ^{14}C exposure ages from this study plotted versus elevation. Note the high ^{10}Be ages, indicative of isotopic inheritance found above 1000 m a.s.l., with lower ages found at lower elevations where glacial erosion was more intense. [Color figure can be viewed at wileyonlinelibrary.com]

demonstrating the lateral advection of material containing high concentrations of cosmogenic nuclides into lower-elevation landscapes dominated by glacial erosion. This process, explored in Hall et al. (2024), notes the importance of erosion, block fracture, and rotation during glacial transport in governing nuclide concentrations in erratic boulders. This, perhaps, provides an analogy to the incorporation of boulders containing inheritance, likely from higher elevation landscapes, into the moraines at Lochain Uaine or Coire an Lochain (Kirkbride et al., 2014). In Lochain Uaine, sampleLU-21-02 appears to have little to no pre-LGM inheritance, as indicated by the similar ^{10}Be and ^{14}C ages. This suggests the sampled surface for LU2102 was either from a shielded bottom or shielded internal surface when entrained, or the material was sourced from a shielded and eroded corrie wall. In contrast, the two samples from the outer moraine at Lochain Uaine appear to contain inherited ^{10}Be, evidenced by divergent ^{14}C and ^{10}Be ages, suggesting the sampled surfaces were derived from rock material that was not entirely shielded from cosmic rays during the last interglacial(s). In total, this highlights the need to use multiple isotopes when employing TCN to reconstruct ice masses in areas within or proximal to regions of low glacial erosion.

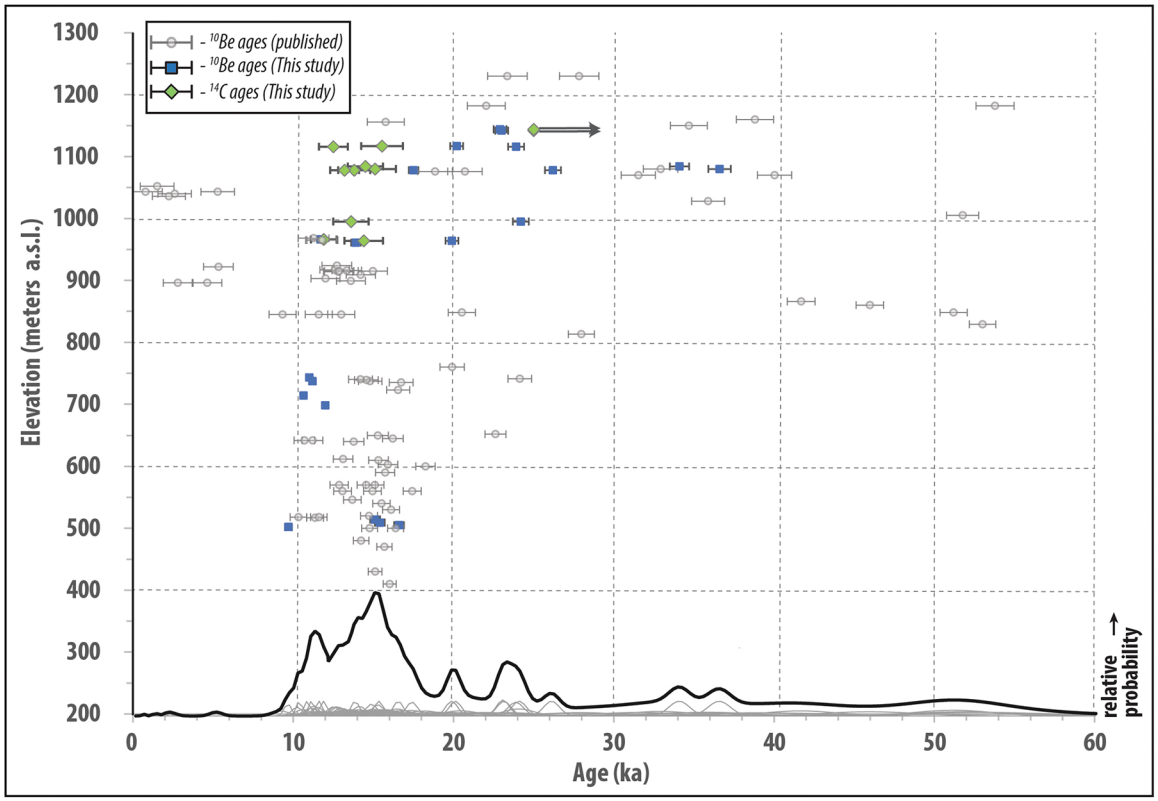

Figure 12. A compilation of 98 exposure ages from the Cairngorm Mountains plotted versus elevation. Blue data points are ^{10}Be ages from this study; green data points are ^{14}C ages from this study, with arrows indicating saturated samples; gray data points are ^{10}Be ages from the published literature. The relative probability of exposure ages is expressed at the bottom of the plot; gray lines are individual samples, and the black curve depicts the summed probability distribution; see Appendix B for sample information. [Color figure can be viewed at wileyonlinelibrary.com]

Conclusions

This study utilizes ^{10}Be and paired ^{10}Be/^{14}C exposure ages to reconstruct the timing and spatial pattern of ice mass fluctuations within the Cairngorm Mountains of central Scotland from the LGM to the Holocene across a 700 m vertical gradient. Our highest elevation samples became ice-free during the LGM. We hypothesize that this is due to dynamic thinning related to BIIS reorganization, although an examination of more high-elevation sites would be needed to test this idea. In the later stages of the Lateglacial, the BIIS and local Cairngorm ice masses were separated. This separation was followed by a readvance of Cairngorm ice at ~15 ka marked by moraines in Glen Derry, as well as on the northern margin of the Cairngorm Mountains. This Cairngorm readvance was coincident with a readvance of the BIIS and deposition of moraines in northwestern Scotland, indicative of a common climatic forcing for either a readvance at 15 ka or synchronous retreat immediately thereafter. Following moraine deposition, ice masses within the Cairngorm Mountains underwent synchronous thinning and marginal retreat in response to Bølling–Allerød warming, with ice masses retreating into the high corries by the YD. The ice marginal retreat was interrupted within corries by stillstands or readvances coincident with Older and Younger Dryas cooling in Glen Derry and Lochain Uaine. The last ice left northward-facing basins in this study at the start of the Holocene, at 11 ka.

We identify clear spatial patterns of cosmogenic nuclide concentrations within samples across an elevational gradient. Samples collected above 1000 m a.s.l., from a landscape lacking clear evidence of glacial erosion, yielded varying amounts of ^{10}Be inheritance with respect to ^{14}C abundances due to variable erosion over past glacial–interglacial cycles. Within high corries, apparent ^{10}Be inheritance was mixed with respect to ^{14}C concentrations, likely owing to the source area and depositional orientation of glacially transported boulders. These findings demonstrate the success of paired ^{10}Be/^{14}C in generating ice mass reconstructions in areas of low-glacial erosion and potential usefulness in resolving paleo-nunataks, an important constraint on past ice sheet thickness.

Acknowledgements. Our fieldwork in the Cairngorms was enabled by the Cairngorm National Park Authority, Cairngorm Mountain, National Trust for Scotland, Mar Lodge Estate, RSPB Abernethy, and NatureScot. Special thanks to Ness Kirkbride, Fiona Cruishank of NatureScot, and Shalia Rao of Mar Lodge for assistance with permitting. We would like to acknowledge the support from our project stakeholder panel: Derek Alexander (NTS Archeology), Ros Bryce (Perth Center Mountain Studies), Kirsty Cameron (Highland), Tom Gardner (HES), Nicki Hall (HES), Ann McSween (NTS), Sophie Nicols (Perth and Kinross), Cath Parker (HES), Daniel Rhodes (NTS Archeology) and Matthew Hawkins (CNPA). Laboratory setup at UCD greatly benefited from discussions with Lee Corbett (U.Vermont) and Alan Hidy (LLNL), the later also provided high quality AMS measurements of ^{10}Be. Field assistance ably provided by Martin Moucheron. PRIME Lab is funded by the US National Science Foundation (EAR-2300559), and we acknowledge AMS assistance from Tom Woodruff. Discussions with Jeremy Ely and Chris Clark at U.Sheffield), and with Adrian Hall and David Sugden at U.Edinburgh improved this manuscript. The Looking Up project was funded by the IRC COALESCE, project 2021/78 awarded to Kelley and Warren.

Data availabilty statement

Data that support the findings of this study are available within the above manuscript; any additional data required is available from the corresponding author upon reasonable request.

Supporting information

Additional supporting information may be found in the online version of this article at the publisher's website.

Appendices Caringorm 2024 revised.

Geo Cairngorm Manuscript supplement-Submit.

References

Balco, G. (2011) Contributions and unrealized potential contributions of cosmogenic-nuclide exposure dating to glacier chronology, 1990–2010. *Quaternary Science Reviews*, 30, 3–27.

Balco, G. (2017) Production rate calculations for cosmic-ray-muon-produced 10Be and 26Al benchmarked against geological calibration data. *Quaternary Geochronology*, 39, 150–173.

Ballantyne, C.K. (1998) Age and significance of mountain-top detritus. *Permafrost and Periglacial Processes*, 9(4), 327–345.

Ballantyne, C.K. (2010) Extent and deglacial chronology of the last British–Irish Ice Sheet: implications of exposure dating using cosmogenic isotopes. *Journal of Quaternary Science*, 25(4), 515–534.

Ballantyne, C.K. & Small, D. (2019) The last Scottish ice sheet. *Earth and Environmental Science Transactions of the Royal Society of Edinburgh*, 110(1–2), 93–131.

Ballantyne, C.K., McCarroll, D. & Stone, J.O. (2006) Vertical dimensions and age of the Wicklow Mountains ice dome, Eastern Ireland, and implications for the extent of the last Irish ice sheet. *Quaternary Science Reviews*, 25(17–18), 2048–2058.

Ballantyne, C.K., Schnabel, C. & Xu, S. (2009b) Readvance of the last British–Irish ice sheet during Greenland interstade 1 (GI-1): the Wester Ross readvance, NW Scotland. *Quaternary Science Reviews*, 28(9–10), 783–789.

Barth, A.M., Clark, P.U., Clark, J., Roe, G.H., Marcott, S.A., McCabe, A.M., et al. (2018) Persistent millennial-scale glacier fluctuations in Ireland between 24 ka and 10 ka. *Geology*, 46(2), 151–154.

Bazin, L., Landais, A., Lemieux-Dudon, B., Toyé Mahamadou Kele, H., Veres, D. & Parrenin, F., et al. (2013) Delta 18O measured on ice core NGRIP on AICC2012 chronology. In: *The Antarctic ice core chronology (AICC2012) [dataset publication series]*. PANGAEA. Available at: https://doi.org/10.1594/PANGAEA.824889.

Beel, C.R., Lifton, N.A., Briner, J.P. & Goehring, B.M. (2016) Quaternary evolution and ice sheet history of contrasting landscapes in Uummannaq and Sukkertoppen, western Greenland. *Quaternary Science Reviews*, 149, 248–258.

Bennett, M.R. & Glasser, N.F. (1991) The glacial landforms of Glen Geusachan, Cairngorms: a reinterpretation. *Scottish Geographical Magazine*, 107(2), 116–123.

Benetti, S., Chiverrell, R.C., Cofaigh, C.Ó., Burke, M., Medialdea, A., Small, D., et al. (2021) Exploring controls of the early and stepped deglaciation on the western margin of the British Irish Ice Sheet. *Journal of Quaternary Science*, 36(5), 833–870.

Borchers, B., Marrero, S., Balco, G., Caffee, M., Goehring, B., Lifton, N., et al. (2016) Geological calibration of spallation production rates in the CRONUS-Earth project. *Quaternary Geochronology*, 31, 188–198.

Bradwell, T., Fabel, D., Stoker, M., Mathers, H., McHargue, L. & Howe, J. (2008) Ice caps existed throughout the Lateglacial Interstadial in northern Scotland. *Journal of Quaternary Science*, 23(5), 401–407.

Bradwell, T., Small, D., Fabel, D., Clark, C.D., Chiverrell, R.C., Saher, M.H., et al. (2021) Pattern, style and timing of British–Irish Ice Sheet retreat: shetland and northern North Sea sector. *Journal of Quaternary Science*, 36(5), 681–722.

Brazier, V., Kirkbride, M.P. & Gordon, J.E. (1998) Active ice-sheet deglaciation and ice-dammed lakes in the northern Cairngorm Mountains, Scotland. *Boreas*, 27(4), 297–310.

Bremmer, A. (1929) The glaciation of the Cairngorms. *The Deeside Field*, 4, 29–37.

Briner, J.P., Lifton, N.A., Miller, G.H., Refsnider, K., Anderson, R. & Finkel, R. (2014) Using in situ cosmogenic 10Be, 14C, and 26Al to decipher the history of polythermal ice sheets on Baffin Island, Arctic Canada. *Quaternary Geochronology*, 19, 4–13.

Briner, J.P., Miller, G.H., Davis, P.T., Bierman, P.R. & Caffee, M. (2003) Last Glacial Maximum ice sheet dynamics in Arctic Canada inferred from young erratics perched on ancient tors. *Quaternary Science Reviews*, 22(5–7), 437–444.

Bromley, G., Putnam, A., Hall, B., Rademaker, K., Thomas, H. & Balter-Kennedy, A., et al. (2023) Lateglacial shifts in seasonality reconcile conflicting North Atlantic temperature signals. *Journal of Geophysical Research: Earth Surface*, 128(1), e2022JF006951.

Brooks, S.J., Matthews, I.P., Birks, H.H. & Birks, H.J.B. (2012) High resolution Lateglacial and early-Holocene summer air temperature records from Scotland inferred from chironomid assemblages. *Quaternary Science Reviews*, 41, 67–82.

Brown, E.J., Rose, J., Coope, R.G. & Lowe, J.J. (2007) An MIS 3 age organic deposit from Balglass Burn, central Scotland: palaeoenvironmental significance and implications for the timing of the onset of the LGM ice sheet in the vicinity of the British Isles. *Journal of Quaternary Science*, 22(3), 295–308.

Butler, M., Cornelissen, M., Nyland, A.J., Posch, C., Kelley, S.E. & Warren, G. (2024) The European Mesolithic in mountain landscapes: comparative perspectives from Austria, Norway, Scotland, and Switzerland. In: Carrer, F., et al. (Eds.) *The Oxford Handbook of Mountain Archaeology*. https://doi.org/10.1093/oxfordhb/9780197608005.013.24

Butler, M., Doughty, A., Lifton, N., Kelley, S., Moucheron, M., O'Brien, C., et al. (2021) Looking Up for prehistoric hunter-gatherer archaeological sites in mountain landscapes in Europe: a case study from the Cairngorms, Scotland. *Hunter Gatherer Research*, 7(3–4), 279–308.

Clark, C.D., Ely, J.C., Hindmarsh, R.C.A., Bradley, S., Ignéczi, A., Fabel, D., et al. (2022) Growth and retreat of the last British–Irish Ice Sheet, 31 000 to 15 000 years ago: the BRITICE-CHRONO reconstruction. *Boreas*, 51(4), 699–758.

Clark, J., McCabe, A.M., Schnabel, C., Clark, P.U., McCarron, S.G. & Freeman, S.P.H.T., et al. (2009) Cosmogenic 10Be chronology of the last deglaciation of western Ireland, and implications for sensitivity of the Irish Ice Sheet to climate change. *Geological Society of America bulletin*, 121(1–2), 3–16.

Corbett, L.B., Bierman, P.R. & Rood, D.H. (2016) An approach for optimizing in situ cosmogenic 10Be sample preparation. *Quaternary Geochronology*, 33, 24–34.

Dalton, A.S., Dulfer, H.E., Margold, M., Heyman, J., Clague, J.J., Froese, D.G., et al. (2023) Deglaciation of the north American ice sheet complex in calendar years based on a comprehensive database of chronological data: NADI-1. *Quaternary Science Reviews*, 321, 108345.

Davis, P.T., Bierman, P.R., Corbett, L.B. & Finkel, R.C. (2015) Cosmogenic exposure age evidence for rapid Laurentide deglaciation of the Katahdin area, west-central Maine, USA, 16 to 15 ka. *Quaternary Science Reviews*, 116, 95–105.

Davis, P.T., Briner, J.P., Coulthard, R.D., Finkel, R.W. & Miller, G.H. (2006) Preservation of Arctic landscapes overridden by cold-based ice sheets. *Quaternary Research*, 65(1), 156–163.

Doughty, A.M., Kelley, S.E., Warren, G., Donebayev, K., Butler, M. & Anderson, B. Modeling Glacier Fluctuations in the Cairngorm Mountains of Scotland during the Lateglacial. *Journal of Quaternary Science*. (in review).

Everest, J. & Golledge, N. (2004) Dating deglaciation in Strathspey and the Cairngorm Mountains. *The Quaternary of the central Grampian Highlands: Field Guide, Quaternary Research Association, Cambridge*, 50–57.

Everest, J. & Kubik, P. (2006) The deglaciation of eastern Scotland: cosmogenic 10Be evidence for a Lateglacial stillstand. *Journal of Quaternary Science*, 21(1), 95–104.

Everest, J.D., Bradwell, T., Fogwill, C.J. & Kubik, P.W. (2006) Cosmogenic 10be age constraints for the wester ross readvance moraine: insights into british ice-sheet behaviour. *Geografiska Annaler: Series A, Physical Geography*, 88(1), 9–17.

Everest, J.D., Bradwell, T., Stoker, M. & Dewey, S. (2013) New age constraints for the maximum extent of the last British–Irish Ice Sheet (NW sector). *Journal of Quaternary Science*, 28, 2–7.

Fabel, D., Ballantyne, C.K. & Xu, S. (2012) Trimlines, blockfields, mountain-top erratics and the vertical dimensions of the last British–Irish Ice Sheet in NW Scotland. *Quaternary Science Reviews*, 55, 91–102.

FitzPatrick, E.A. (1965) An interglacial soil at Teindland, Morayshire. *Nature*, 207(4997), 621–622.
Goehring, B.M., Brown, N., Moon, S. & Blisniuk, K. (2021) The transport history of alluvial fan sediment inferred from multiple geochronometers. *Journal of Geophysical Research: Earth Surface*, 126(9), e2021JF006096.
Golledge, N. (2002) Glaci-tectonic deformation of proglacial lake sediments in the Cairngorm Mountains. *Scottish Journal of Geology*, 38(2), 127–136.
Golledge, N.R., Hubbard, A. & Sugden, D.E. (2008) High-resolution numerical simulation of Younger Dryas glaciation in Scotland. *Quaternary Science Reviews*, 27(9–10), 888–904.
Gosse, J.C. & Phillips, F.M. (2001) Terrestrial in situ cosmogenic nuclides: theory and application. *Quaternary Science Reviews*, 20(14), 1475–1560.
Graham, A., Lonergan, L. & Stoker, M. (2007) Evidence for Late Pleistocene ice stream activity in the Witch Ground Basin, central North Sea, from 3D seismic reflection data. *Quaternary Science Reviews*, 26(5–6), 627–643.
Graham, B.L., Briner, J.P., Schweinsberg, A.D., Lifton, N.A. & Bennike, O. (2019) New in situ 14C data indicate the absence of nunataks in west Greenland during the Last Glacial Maximum. *Quaternary Science Reviews*, 225, 105981.
Gump, D.J., Briner, J.P., Mangerud, J. & Svendsen, J.I. (2017) Deglaciation of Boknafjorden, south-western Norway. *Journal of Quaternary Science*, 32(1), 80–90.
Hall, A.M. & Phillips, W.M. (2006) Glacial modification of granite tors in the Cairngorms, Scotland. *Journal of Quaternary Science*, 21(8), 811–830.
Hall, A.M. & Sugden, D.E. (1987) Limited modification of mid-latitude landscapes by ice sheets: the case of northeast Scotland. *Earth surface processes and landforms*, 12(5), 531–542.
Hall, A.M., Binnie, S.A., Sugden, D., Dunai, T.J. & Wood, C. (2016) Late readvance and rapid final deglaciation of the last ice sheet in the Grampian Mountains, Scotland. *Journal of Quaternary Science*, 31(8), 869–878.
Hall, A.M., Gillespie, M.R., Thomas, C.W. & Ebert, K. (2013) Scottish landform examples: the Cairngorms–a pre-glacial upland granite landscape. *Scottish Geographical Journal*, 129(1), 2–14.
Hall, A.M., Sugden, D.E., Binnie, S.A., Hein, A., Dunai, T., Ritter, B., et al. (2024) Inherited terrestrial cosmogenic nuclides in landscapes of selective glacial erosion: lessons from Lochnagar, Eastern Grampian Mountains, Scotland. *Journal of Quaternary Science*, 39(4), 515–530.
Hall, B.L., Borns Jr., H.W., Bromley, G.R.M. & Lowell, T.V. (2017) Age of the Pineo Ridge System: implications for behavior of the Laurentide Ice Sheet in eastern Maine, USA, during the last deglaciation. *Quaternary Science Reviews*, 169, 344–356.
Harrison, T.N. (1988) Magmatic garnets in the Cairngorm granite, Scotland. *Mineralogical Magazine*, 52(368), 659–667.
Hättestrand, C. & Stroeven, A.P. (2002) A relict landscape in the centre of Fennoscandian glaciation: geomorphological evidence of minimal Quaternary glacial erosion. *Geomorphology*, 44(1–2), 127–143.
Hibbert, F.D., Austin, W.E.N., Leng, M.J. & Gatliff, R.W. (2010) British Ice Sheet dynamics inferred from North Atlantic ice-rafted debris records spanning the last 175 000 years. *Journal of Quaternary Science*, 25(4), 461–482.
Hippe, K. & Lifton, N.A. (2014) Calculating isotope ratios and nuclide concentrations for in situ cosmogenic 14C analyses. *Radiocarbon*, 56(3), 1167–1174.
Hubbard, A., Bradwell, T., Golledge, N., Hall, A., Patton, H., Sugden, D., et al. (2009) Dynamic cycles, ice streams and their impact on the extent, chronology and deglaciation of the British–Irish ice sheet. *Quaternary Science Reviews*, 28(7–8), 758–776.
Hughes, A.L.C., Clark, C.D. & Jordan, C.J. (2014) Flow-pattern evolution of the last British Ice Sheet. *Quaternary Science Reviews*, 89, 148–168.
Hughes, P.D., Glasser, N.F. & Fink, D. (2022) 10Be and 26Al exposure history of the highest mountains in Wales: evidence from Yr Wyddfa (Snowdon) and Y Glyderau for a nunatak landscape at the global Last Glacial Maximum. *Quaternary Science Reviews*, 286, 107523.
Huntley, B. (1976) *The Past and Present Vegetation of the Morrone Birkwoods and Caenlochan National Nature Reserves*. Cambridge: University of Cambridge.
Ives, J.D. (1978) The maximum extent of the Laurentide Ice Sheet along the east coast of North America during the last glaciation. *Arctic*, 31, 24–53.
Jamieson, T.F. (1908) A geologist on the Cairngorms. *Cairngorm Club Journal*, 5, 82–88.
Johnson, J.S., Nichols, K.A., Goehring, B.M., Balco, G. & Schaefer, J.M. (2019) Abrupt mid-Holocene ice loss in the western Weddell Sea Embayment of Antarctica. *Earth and Planetary Science Letters*, 518, 127–135.
Kelley, S.E., Briner, J.P., Young, N.E., Babonis, G.S. & Csatho, B. (2012) Maximum late Holocene extent of the western Greenland Ice Sheet during the late 20th century. *Quaternary Science Reviews*, 56, 89–98. Available from: https://doi.org/10.1016/j.quascirev.2012.09.016
Kirkbride, M., Everest, J., Benn, D., Gheorghiu, D. & Dawson, A. (2014) Late-Holocene and Younger Dryas glaciers in the northern Cairngorm Mountains, Scotland. *The Holocene*, 24(2), 141–148.
Kirkbride, V. & Gordon, J.E. (2010) *The geomorphological heritage of the Cairngorm Mountains*. Scottish Natural Heritage.
Kleman, J. (1994) Preservation of landforms under ice sheets and ice caps. *Geomorphology*, 9(1), 19–32.
Koester, A.J. & Lifton, N.A. (2023) Technical note: a software framework for calculating compositionally dependent in situ 14C production rates. *Geochronology*, 5(1), 21–33.
Koester, A.J. & Lifton, N.A. (2024) *Corrigendum* to "Technical note: a software framework for calculating compositionally dependent in situ14C production rates". Published in *Geochronology*, 5, 21–33. Available from: https://doi.org/10.5194/gchron-5-21-2023-corrigendum
Koester, A.J., Shakun, J.D., Bierman, P.R., Davis, P.T., Corbett, L.B. & Goehring, B.M., et al. (2021) *Laurentide ice sheet thinning and erosive regimes at Mount Washington, New Hampshire, inferred from multiple cosmogenic nuclides*. Colorado: Geological Society of America.
Koester, A.J., Shakun, J.D., Bierman, P.R., Davis, P.T., Corbett, L.B., Braun, D., et al. (2017) Rapid thinning of the Laurentide Ice Sheet in coastal Maine, USA, during late Heinrich Stadial 1. *Quaternary Science Reviews*, 163, 180–192.
Landmap GetMapping (2014) GetMapping 5m resolution Digital Terrain Model (DTM) for Scotland. NERC Earth Observation Data Centre. Available from: https://catalogue.ceda.ac.uk/uuid/fe89226774e191a45ea4a17c4d64cea1/ [Accessed 28th March 2025].
Lifton, N. (2016) Implications of two Holocene time-dependent geomagnetic models for cosmogenic nuclide production rate scaling. *Earth and Planetary Science Letters*, 433, 257–268.
Lifton, N., Sato, T. & Dunai, T.J. (2014) Scaling in situ cosmogenic nuclide production rates using analytical approximations to atmospheric cosmic-ray fluxes. *Earth and Planetary Science Letters*, 386, 149–160.
Lifton, N., Wilson, J. & Koester, A. (2023) Technical note: studying lithium metaborate fluxes and extraction protocols with a new, fully automated in situ cosmogenic 14C processing system at PRIME Lab. *Geochronology*, 5(2), 361–375.
Margold, M., Stokes, C.R. & Clark, C.D. (2015) Ice streams in the Laurentide Ice Sheet: identification, characteristics and comparison to modern ice sheets. *Earth-Science Reviews*, 143, 117–146.
McCarroll, D. (2016) Trimline trauma: the wider implications of a paradigm shift in recognising and interpreting glacial limits. *Scottish Geographical Journal*, 132(2), 130–139.
McCarroll, D., Ballantyne, C.K., Nesje, A. & DAHL, S.O. (1995) Nunataks of the last ice sheet in northwest Scotland. *Boreas*, 24(4), 305–323.
McMartin, I., Godbout, P.M., Campbell, J.E., Tremblay, T. & Behnia, P. (2021) A new map of glacigenic features and glacial landsystems in central mainland Nunavut, Canada. *Boreas*, 50(1), 51–75.
Merritt, J.W., Connell, E.R. & Hall, A.M. (2017) Middle to Late Devensian glaciation of north-east Scotland: implications for the northeastern quadrant of the last British–Irish Ice Sheet. *Journal of Quaternary Science*, 32(2), 276–294.
Microsoft Virtual Earth (2025) Bing Maps Aerial Basemap for ArcGIS. Available at: https://www.bing.com/maps [Acessed 28th March 2025].
Morley, A., de la Vega, E., Raitzsch, M., Bijma, J., Ninnemann, U. & Foster, G.L., et al. (2024) A solution for constraining past marine Polar Amplification. *Nature Communications*, 15(1), 1–12. Available from: https://doi.org/10.1038/s41467-024-53424-w

Nichols, K.A., Goehring, B.M., Balco, G., Johnson, J.S., Hein, A.S. & Todd, C. (2019) New last glacial maximum ice thickness constraints for the Weddell Sea Embayment, Antarctica. *The Cryosphere*, 13(11), 2935–2951.

Nygård, A., Sejrup, H.P., Haflidason, H., Cecchi, M. & Ottesen, D. (2004) Deglaciation history of the southwestern Fennoscandian Ice Sheet between 15 and 13 14C ka BP. *Boreas*, 33(1), 1–17. Available from: https://doi.org/10.1111/j.1502-3885.2004.tb00992.x

Pendleton, S., Miller, G., Lifton, N. & Young, N. (2019a) Cryosphere response resolves conflicting evidence for the timing of peak Holocene warmth on Baffin Island, Arctic Canada. *Quaternary Science Reviews*, 216, 107–115.

Pendleton, S.L., Miller, G.H., Lifton, N., Lehman, S.J., Southon, J., Crump, S.E. et al. (2019b) Rapidly receding Arctic Canada glaciers revealing landscapes continuously ice-covered for more than 40,000 years. *Nature communications*, 10(1), 445.

Phillips, W.M., Hall, A.M., Mottram, R., Fifield, L.K. & Sugden, D.E. (2006) Cosmogenic 10Be and 26Al exposure ages of tors and erratics, Cairngorm Mountains, Scotland: timescales for the development of a classic landscape of selective linear glacial erosion. *Geomorphology*, 73(3–4), 222–245.

Prest, V., Grant, D. & Rampton, V. (1967) Glacial map of Canada: Geological Survey of Canada. Map 1253A:(Scale 1: 5 000 000).

Rae, A.C., Harrison, S., Mighall, T. & Dawson, A.G. (2004) Periglacial trimlines and nunataks of the Last Glacial Maximum: the Gap of Dunloe, southwest Ireland. *Journal of Quaternary Science*, 19(1), 87–97.

Rapson, S.C. (1983) *The age of corrie moraines and postglacial environmental change in the Cairngorm Mountains*. Scotland: University of Aberdeen (United Kingdom).

Rea, B.R. (1998) The Cairngorms—a landscape of selective linear erosion. *Scottish Geographical Magazine*, 114(2), 124–129.

Reimer, P.J. (2020) Composition and consequences of the IntCal20 radiocarbon calibration curve. *Quaternary Research*, 96, 22–27.

Roberts, D.H., Evans, D.J.A., Callard, S.L., Clark, C.D., Bateman, M.D., Medialdea, A., et al. (2018) Ice marginal dynamics of the last British-Irish Ice Sheet in the southern North Sea: ice limits, timing and the influence of the Dogger Bank. *Quaternary Science Reviews*, 198, 181–207.

Robinson, M. & Ballantyne, C.K. (1979) Evidence for a glacial readvance pre-dating the Loch Lomond Advance in Wester Ross. *Scottish Journal of Geology*, 15(4), 271–277.

Rootes, C.M. & Clark, C.D. (2020) Glacial trimlines to identify former ice margins and subglacial thermal boundaries: a review and classification scheme for trimline expression. *Earth-Science Reviews*, 210, 103355.

Scourse, J.D. (2024) The timing and magnitude of the British–Irish Ice Sheet between Marine Isotope Stages 5d and 2: implications for glacio-isostatic adjustment, high relative sea levels and 'giant erratic' emplacement. *Journal of Quaternary Science*, 39(4), 505–514.

Sejrup, H.P., Clark, C.D. & Hjelstuen, B.O. (2016) Rapid ice sheet retreat triggered by ice stream debuttressing: evidence from the North Sea. *Geology*, 44(5), 355–358.

Sissons, J.B. (1979) The Loch Lomond Advance in the Cairngorm Mountains. *Scottish Geographical Magazine*, 95(2), 66–82.

Sissons, J.B. & Walker, M.J.C. (1974) Late glacial site in the central Grampian Highlands. *Nature*, 249(5460), 822–824.

Spector, P., Stone, J., Balco, G., Hillebrand, T., Thompson, M. & Black, T. (2020) Miocene to Pleistocene glacial history of West Antarctica inferred from Nunatak geomorphology and cosmogenic-nuclide measurements on bedrock surfaces. *American Journal of Science*, 320(8), 637–676.

Standell, M.R. (2014) *Lateglacial (Younger Dryas) glaciers and ice-sheet deglaciation in the Cairngorm Mountains, Scotland: glacier reconstructions and their palaeoclimatic implications*. London: Loughborough University.

Steffensen, J.P., Andersen, K.K., Bigler, M., Clausen, H.B., Dahl-Jensen, D., Fischer, H., et al. (2008) High-resolution Greenland ice core data show abrupt climate change happens in few years. *Science*, 321(5889), 680–684.

Stroeven, A.P., Fabel, D., Hättestrand, C. & Harbor, J. (2002) A relict landscape in the centre of Fennoscandian glaciation: cosmogenic radionuclide evidence of tors preserved through multiple glacial cycles. *Geomorphology*, 44(1–2), 145–154.

Sugden, D.E. (1968) The selectivity of glacial erosion in the Cairngorm Mountains, Scotland. *Transactions of the Institute of British Geographers*, 45, 79–92.

Sugden, D.E. (1970) Landforms of deglaciation in the Cairngorm Mountains, Scotland. *Transactions of the Institute of British Geographers*, 51, 201–219.

Sugden, D.E. (1978) Glacial erosion by the Laurentide ice sheet. *Journal of Glaciology*, 20(83), 367–391.

Sugden, D. & Hall, A. (2020) Antarctic blue-ice moraines: analogue for Northern Hemisphere ice sheets? *Quaternary Science Reviews*, 249, 106620.

Svensson, A., Andersen, K.K., Bigler, M., Clausen, H.B., Dahl-Jensen, D., Davies, S.M., et al. (2008) A 60 000 year Greenland stratigraphic ice core chronology. *Climate of the Past*, 4(1), 47–57.

Vasari, Y. & Vasari, A. (1968) Late- and post-glacial macrophytic vegetation in the lochs of northern Scotland. *Acta Botanica Fennica*, 80, 120. https://helda.helsinki.fi/items/ff385c4d-1086-4953-a9b3-f9af95773544

Voelker, A.H., Sarnthein, M., Grootes, P.M., Erlenkeuser, H., Laj, C., Mazaud, A., et al. (1997) Correlation of marine 14C ages from the Nordic Seas with the GISP2 isotope record: implications for 14C calibration beyond 25 ka BP. *Radiocarbon*, 40(1), 517–534.

Whittington, G. & Hall, A.M. (2002) The Tolsta Interstadial, Scotland: correlation with D–O cycles GI-8 to GI-5? *Quaternary Science Reviews*, 21(8–9), 901–915.

Wickham-Jones, C., Noble, G., Fraser, S., Warren, G., Tipping, R. & Paterson, D., et al. (2020) New evidence for upland occupation in the Mesolithic of Scotland. *Proceedings of the Prehistoric Society*, 86, 13–42.

Young, N.E., Briner, J.P., Schaefer, J.M., Miller, G.H., Lesnek, A.J., Crump, S.E., et al. (2020) Reply to Carlson (2020) comment on "Deglaciation of the Greenland and Laurentide ice sheets interrupted by glacier advance during abrupt coolings". *Quaternary Science Reviews*, 240, 106329.

Young, N.E., Schaefer, J.M., Goehring, B., Lifton, N., Schimmelpfennig, I. & Briner, J.P. (2014) West Greenland and global in situ 14C production-rate calibrations. *Journal of Quaternary Science*, 29(5), 401–406.